Institut für Veterinärbiochemie und Molekularbiologie
der Vetsuisse-Fakultät Universität Zürich

Direktor: Prof. Ulrich Hübscher
Abteilungsleiter: Prof. Michael O. Hottiger

Arbeit unter Leitung von Dr. Paul O. Hassa

Identification of p62 as interaction partner of ARTD9 – is ARTD9 degraded by autophagy?

Inaugural-Dissertation

zur Erlangung der Doktorwürde der
Vetsuisse-Fakultät Universität Zürich

vorgelegt von

Hans Christian Winkler

Tierarzt
von Zürich und Basel, Schweiz

genehmigt auf Antrag von

Prof. Michael O. Hottiger, Referent

Prof. Hanspeter Nägeli, Korreferent

Zürich 2012

Table of Content

Summary

B-aggressive lymphoma 1 protein (BAL1/ARTD9) was described as prognostic marker for the progression of diffuse large B-cell lymphoma, the most common lymphoid cancer in humans. As a *macro*ARTD, BAL1/ARTD9 contains 2 *macro* and an ADP-ribosyltransferase domain, the signature of diphteria toxin-like ADP-ribosyltransferases (ARTDs). The aim of this study was to identify and functionally characterize interaction partners of the *macro*ARTD proteins. Using an unbiased glutathione S-transferase (GST) pull-down and co-immunoprecipitation approach, full length and *macro* domain specific interaction partners of BAL complexes were investigated under physiological conditions. Subsequently, protein interaction partners were identified by mass spectrometry and validated by western blot. Among other proteins, p62, a signaling hub involved in selective autophagy, was found as specific interaction partner of the ARTD9 *macro* domains. p62 is up-regulated in several human tumors. Therefore the effect of autophagy induction on ARTD9 was investigated. We discovered that ARTD9 levels are decreased upon induction of autophagy by starvation in A549 cells. This effect was abolished by p62 but not beclin-1 siRNA. These results revealed that ARTD9 is degraded by p62 dependent but beclin-1 independent selective autophagy.

Zusammenfassung

Das B-aggressive Lymphomprotein (BAL1/ARTD9) wurde als prognostischen Marker für den Verlauf von diffus grosszelligem B-Zell Lymphom identifiziert, dem meistdiagnostizierten Lymphom bei Erwachsenen. Als *macro*ARTD enthält ARTD9 zwei *macro* Domänen und eine ADP-ribosyl-transferasen-Domäne, und gehört somit zu den diphterietoxin-ähnlichen ADP-ribosyltransferasen (ARTDs). Ziel dieser Arbeit war es, Interaktionspartner von *macro*ARTD Proteinen zu identifizieren und funktionell zu charakterisieren. Unter Verwendung eines unvoreingenommenen Immunpräzipitationsverfahrens und mit Hilfe von Glutathion S-Transferase (GST) Pulldowns wurden Interaktionspartner der gesamtprotein- als auch der *macro*-Domänen-spezifischen BAL-Komplexe unter physiologischen Bedingungen untersucht. Anschliessend wurden interagierende Proteine mit Massenspektrometrie identifiziert und mittels Westernblot validiert. Das Protein p62, das an der selektiven Autophagie zentral beteiligt ist, wurde als spezifischer Interaktionspartner der ARTD9 *macro* Domänen gefunden. p62 ist in mehreren menschlichen Tumoren hochreguliert. Daher wurde der Effekt induzierter Autophagie auf ARTD9 untersucht. Wir stellten fest, dass die Menge an ARTD9 abnimmt, wenn Autophagie durch Hungern in A549 Zellen ausgelöst wird. Dieser Effekt konnte mit p62 siRNA aufgehoben werden, jedoch nicht mit beclin-1 siRNA. Diese Resultate zeigen, dass ARTD9 durch p62 abhängige aber beclin-1 unabhängige selektive Autophagie abgebaut wird.

Abbreviations

293T	Human embryonic kidney cell line
7B	*Macro* domain B of ARTD7
8C	*Macro* domain C of ARTD8
9B	*Macro* domain B of ARTD9
9Tm	Tandem *macro* domains of ARTD9
A549	Human type II bronchial epithelial carcinoma cell line
ADP	Adenosine diphosphate
ADPr	ADP-ribose
ADPRT	ADP-ribosyltransferase domain
AF1521	*Macro* domain of *A. fulgidus*
AMP	Adenosine monophosphate
AMPK	5' AMP-activated protein kinase
ARTD	ADP-ribosyltransferase diphteria toxin-like
Atg	Autophagy related genes
ATP	Adenosine triphosphate
BAL	B aggressive lymphoma
BBAP	B-lymphoma- and BAL-associated protein
BCL	B-cell lymphoma protein
BSA	Bovine serum albumin
CD	Cluster of differentiation
CMA	Chaperone-mediated autophagy
DLBCL	Diffuse large B-cell lymphoma
DMEM	Dulbecco's modified Eagle's medium
DNA	Desoxyribonucleic acid
EtBr	Ethidium bromide
EtOH	Ethanol
ER	Endoplasmic reticulum
FBS	Fetal bovine serum
FL	Full length
GST	Glutathione S-transferase
HA	Hemagglutinin
IFN	Interferon

IL	Interleukin
IRF	Interferon regulatory factor
ISGF	Interferon-stimulated gene factor
JAK	Janus kinase
kD	Kilodalton
LC3	Microtubule-associated protein light chain 3
LB	Luria Bertani
LPS	E. coli lipopolysaccharide
MART	Mono(ADP-ribosyl) transferase
mD2	*Macro* domain of macro domain containing protein 2
mH2A1.1	*Macro* domain of histone variant macroH2A1.1
MSA	Multiple sequence alignment
mTORC1	Mammalian target of rapamycin complex 1
NAD^+	Nicotinamide adenine dinucleotide
NHL	Non-Hodgkin lymphoma
OAADPr	O-acetyl-ADP-ribose
PAGE	Polyacrylamide gel electrophoresis
PAR	Poly(ADP-ribose) polymer
PARP	Poly(ADP-ribose) polymerase
PBS	Phosphate-buffered saline
PCR	Polymerase chain reaction
PI3K	Phosphoinositide-3-OH kinase
PIAS	Protein inhibitors of activated STATs
PIK3C3	Class III phosphatidylinositol-3-OH kinase complex
PKC	Protein kinase C
poly(A)	Poly(adenosine monophosphate)
PtdIns(3)P	Phosphatidylinositol-3-phosphate
PTEN	Phosphatase and tensin homolog on chromosome ten
PTM	Post-translational modification
RAW-264.7	Mouse monocyte/macrophage cell line
RNA	Ribonucleic acid
RPMI-1640	Roswell Park Memorial Institute 1640 medium
RT	reverse transcribed
p70S6K	70kDa protein S6 kinase
SDS	Sodium dodecyl sulfate
shRNA	Short hairpin RNA
SLIM	STAT-interacting LIM protein
SOCS	Suppressor of cytokine signaling
ssRNA	Single-stranded RNA
STAT	Signal transducer and activator of transcription

SUDHL7	Uncharacterized human B-cell line
TBS	Tris-buffered saline
TBST	Tris-buffered saline Tween® 20
U-2932	Human diffuse large B-cell lymphoma cell line
ULK1	Unc-51-like kinase 1
WBC	White blood cell
WCE	Whole cell extracts

Units

℃	Degrees Celsius
Da	Dalton
h	Hour
L	Liter
min	Minute
rpm	Revolutions per Minute
U	Unit

1 Introduction

Protection of a host against pathogens and tumor cells is crucial for its survival. The vertebrate immune system achieves this with three layers: 1. a mechanical/physical barrier working continuously, 2. innate immunity that reacts within hours and 3. adaptive immunity to target invaders specifically within several days. To avoid invading pathogens, i.e. infectious diseases, the immune system reacts rapidly and tightly coordinated. Overreaction of inflammation and immunity can harm the host, therefore homeostasis between activation and suppression of the defense mechanisms is key for survival (1). Aberrant signaling often leads to chronic inflammatory disorders and cancer (2). Post-translational modifications (PTMs) are a fast, accurate and reversible way to regulate signaling and transcription. These modifications include phosphorylation, acetylation, methylation, ubiquitination and adenosine diphosphate ribosylation (ADP-ribosylation) (3–5). Another key regulator of inflammation and immunity proteins is the autophagy signaling pathway (6–9).

1.1 The family of intracellular diphteria toxin-like mono- and polymerizing-ADP-ribosyltransferases

ADP-ribosylation is the enzymatic transfer of the ADP-ribose moiety from nicotinamide adenine dinucleotide (NAD^+) onto acceptor amino acid side chains and/or ADP-ribose units bound to target proteins. A schematic representation of the mono-ADP-ribosylation process of an asparagine is shown in Fig. 1.

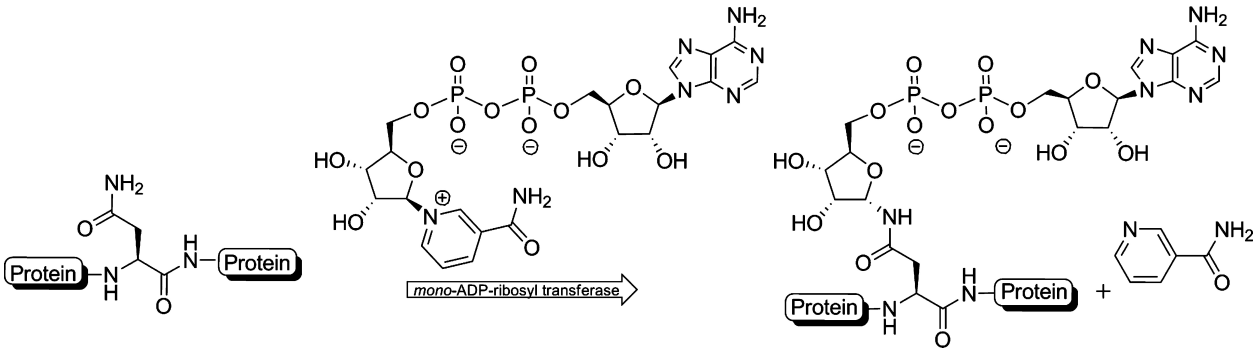

Figure 1. Mono-ADP-ribosylation of a protein at an asparagine residue. From (10)

ADP-ribosylation is mediated by mono- and poly-ADP-ribosyltransferases (11). These enzymes contain an active site with similarities to diphtheria toxin and are therefore known as diphtheria toxin-like ADP-ribosyltransferases (ARTDs) (12). In humans, 17 members of the ARTD family have been found, all of which contain an ADP-ribosyltransferase (ADPRT) domain also referred to as catalytic domain (12, 13). Three family members, ARTD7/B aggressive lymphoma protein 3 (BAL3), ARTD8/BAL2 and ARTD9/BAL1, contain multiple N-terminal *macro* domains (14). These three proteins, termed *macro*ARTDs, are conserved in many eukaryotic species, with the exception of rodents, which lack ARTD7. The *macro*ARTD genes are located on the human chromosome 3q21 and form a cluster (15). ARTD8 and ARTD9 are expressed during mouse development and adulthood prominently in the thymus (16). The *macro*ARTDs ARTD7 and ARTD8 were shown to be mono-ADP-ribosyltransferases. The ADPRT domain of ARTD9 is probably inactive, due to amino acid substitutions in the histidine, tyrosine and glutamate (HYE) triad of the catalytic domain. Instead, it contains the motif glutamine, tyrosine and threonine (QYT) (14, 17, 18).

Another domain present in ARTD8 is the WWE domain (named after the conserved tryptophans and a glutamic acid), predicted to be a protein-protein interaction module necessary for targeted ubiquitination and ADP-ribosylation (19). Recently, this domain was reported to bind *iso*-ADP-ribose and poly(ADP-ribose) polymer (PAR) (20). A schematic representation of the domain structure of ARTD7–9/BAL1–3 and the respective *macro* domains expressed during this study as His-GST fusions is shown in Fig. 2.

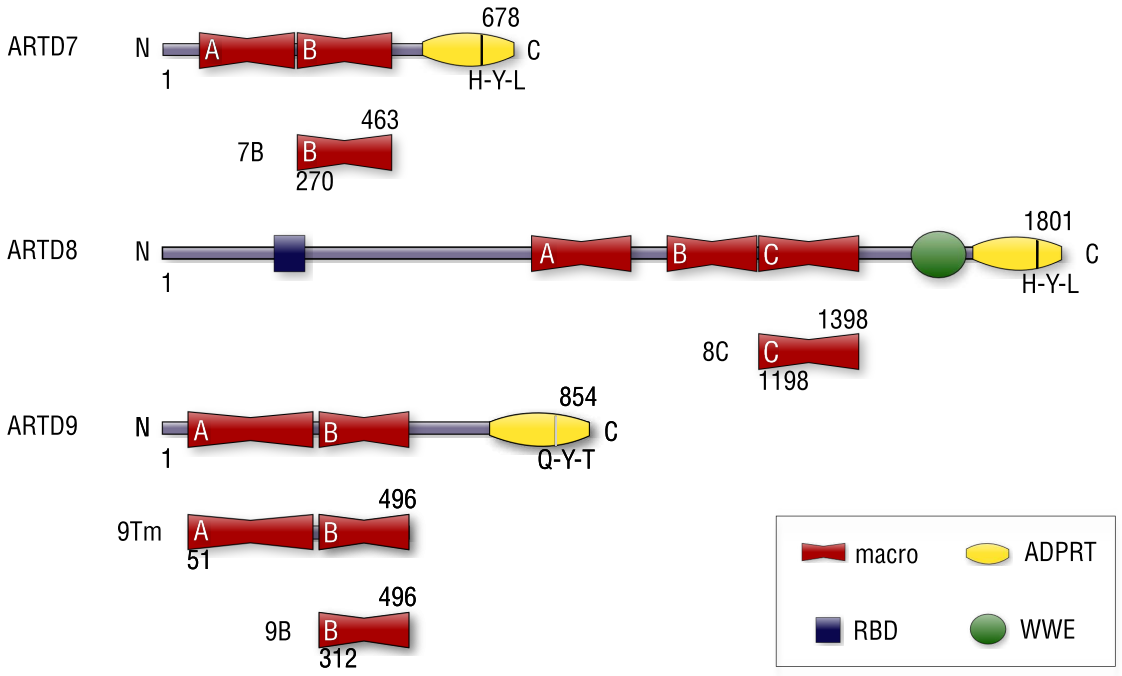

Figure 2. Schematic representation of human ARTD7–9/BAL1–3 proteins and the recombinantly expressed *macro* domains. The amino acids at the positions of the HYE triad of ARTD1 are indicated below the catalytic domains.

1.1.1 *Macro* domains are ADP-ribose-binding protein modules

Using a multiple sequence alignment (MSA), A. E. Gorbalenya, E. V. Koonin and M. M.-C. Lai discovered that the domain with the highest similarity in α- and rubivirus is also conserved in coronaviruses and denoted it X domain (21, 22). Shortly after, J. R. Pehrson and V. A. Fried isolated and cloned the histone variant macroH2A that is almost three times as large as canonical histone H2A. MacroH2A is associated with transcriptional repression and X chromosome inactivation (23). It contains a carboxy-terminal non-histone segment, termed *macro* domain (24). Alignment of these domains suggested that they constitute the same family. Therefore, the *macro* or X domain is a phylogenetically ancient and highly conserved protein module found in proteins of several eukaryotic and prokaryotic species as well as in positive-stranded RNA viruses. Several *macro* domains were shown to bind the NAD^+ metabolites poly(ADP-ribose) polymer (PAR) , monomeric ADP-ribose (ADPr) and the sirtuin metabolite O-acetyl-ADP-ribose (OAADPr).

Additionally, several mammalian and bacterial *macro* domain proteins had phosphatase activity and were able to hydrolyze ADPr-1"-phosphate, a by-product of tRNA splicing (25–30).

Viral *macro* domains are found in all viruses of the *Coronaviridae* family, in Rubella viruses, Alpha viruses and Hepatitis E virus (22, 31). Viral *macro* domains were shown to bind to bind PAR as well as poly(A) (29, 32). The bacterial *macro* domain-only protein AF1521 was shown to bind the NAD^+ metabolites PAR, ADPr and OAADPr (33).

MacroH2A has been associated with the inactive X chromosome in female mammals and is implicated in transcriptional regulation in vertebrates. In mammals, macroH2A2 and two splicing variants of macroH2A1 exist (34). Of the three mammalian macroH2A isoforms macroH2A1.1, macroH2A1.2 and macroH2A2, only macroH2A1.1 is able to bind PAR, ADPr and the sirtuin metabolite OAADPr (35). In contrast, the human macroD2, was found to reside in both nucleus and cytoplasm, possibly shuttling, and binding specifically to monomeric ADPr with high affinity (Kd = 0.15 μM). However, it did not bind PAR efficiently (29). Since endogenous ARTD1 is poly- and mono-ADP-ribosylated as well (36, 37), several *macro* domain containing proteins bind ARTD1, for example AF1521, ALC1 and mH2A1.1 (33, 35, 36, 38).

*Macro*ARTDs are so far the only proteins characterized, that contain multiple *macro* domains. The *macro* domains of ARTD7, ARTD8 and ARTD9 are conserved, but contrary to expectations, the intermolecular similarities are higher than the intramolecular evolutionary conservation (14). The evolutionary tree of the *macro* domains of ARTD7, ARTD8 and ARTD9 is shown in Fig. 3.

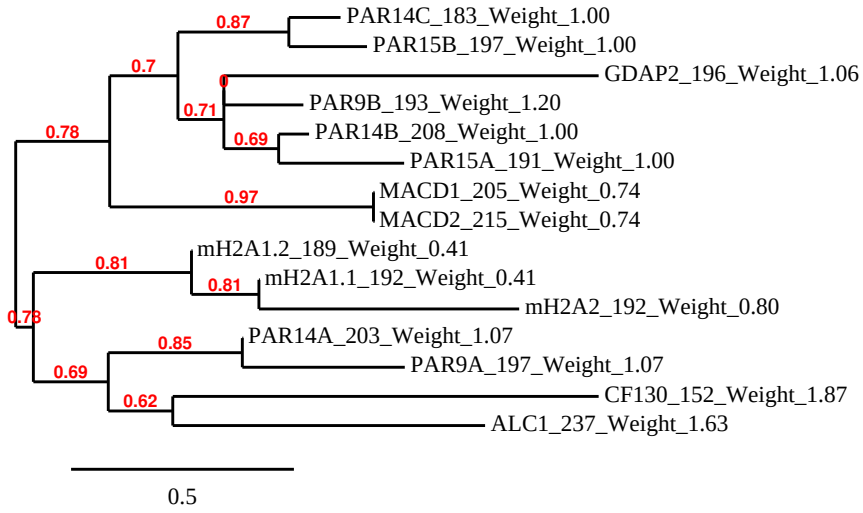

Figure 3. The evolutionary tree of the human *macro* domains. PAR14 indicates ARTD8, PAR15 ARTD7 and PAR9 ARTD9. The intermolecular similarity between the *macro* domains of ARTD7–ARTD9 is higher then the intramolecular similarity. Personal communication, M. Hassler (EMBL, Heidelberg).

1.1.2 General roles of ARTD9/BAL1 and ARTD8/BAL2 in immunity and tumorigenesis

ARTD9/B-aggressive lymphoma 1 (BAL1) has been discovered in a genome-wide screen as candidate gene, whose expression correlates with risk and chemoresistance in diffuse large B-cell lymphoma (DLBCL) (15). In a recent microarray study, ARTD9 was shown to be significantly upregulated upon signal transducer and activator of transcription 6 (STAT6) knockdown (STAT6 acts downstream of interleukin 4 (IL-4), cf. section 1.2 below) by short hairpin RNA (shRNA) in a classical Hodgkin lymphoma cell line (39). BAL2/ARTD8, another member of the same family, is suggested to be a transcriptional activator/switch for STAT6 (40, 41). It was shown to protect against apoptosis in IL-4 treated cells (42) IL-4 inhibits Th1 response and IFNγ production, while IFNγ inhibits Th2 response, as mentioned below (section 1.2). Therefore the discovery that ARTD9 and B-lymphoma- and BAL-associated protein (BBAP) are regulated by the same interferon-responsive bidirectional promoter (43) indicates, that ARTD9 and ARTD8 act in an antagonistic way.

1.1.3 Specific Roles of the ARTD9/BAL1 as modulator of STAT1/IRF1 in tumorigenesis

In our lab, ARTD9 was found as a co-activator of STAT1 and repressor for tumor suppressor interferon regulatory factor 1 (IRF1) in SUDHL7 DLBCL cells. Meanwhile, it stimulated the expression of the proto-oncogenes B-cell lymphoma 6 (BCL6), BCL2 and IRF2 in these cells. ARTD9/BAL1

bound to the IRF1 promoter as well as its own promoter. ARTD9/BAL1 physically interacts with both STAT1α and STAT1β through its macro domains (44).

1.2 General roles of interferons in innate immunity and tumorigenesis

Adaptive immunity is mediated by lymphocytes (B- and T-cells) through the production of cytokines. These small secreted mediators control differentiation, proliferation and apoptosis of white blood cells (WBCs) and other cells of hematopoetic origin (45, 47). A major trigger of the immune response is the equilibrium between type 1 T helper CD4+ cells (Th1) and type 2 T helper CD4+ cells (Th2). A hallmark of Th1 or *inflammatory T cells* is the production of interferon γ (IFNγ), which activates macrophages and stimulates an inflammatory response. The Th1 response is important for defense against intracellular bacteria, viruses and cancerous cells and is necessary for type IV hypersensitivity. Conversely, the cytokine interleukin 4 (IL-4) shifts the immune system towards Th2 response, also called *humoral immunity*. This immune response is responsible for the production of high affinity antibodies against extracellular pathogens. IL-4 promotes activated B-cells to proliferate and induces activation-induced deaminase, which is required for class switch recombination to the IgE isotype and somatic hypermutation. Since IL-4 inhibits Th1 response and IFNγ production and *vice versa*, Th1 and Th2 response act in an antagonistic way (48).

IFNs and IL-4 elicit their functions through binding to transmembrane receptors. Receptor associated Janus kinase (JAK) subsequently phosphorylates cytoplasmic signal transducer and activator of transcription (STAT) on tyrosine residues. Upon IL-4 binding to the IL-4/IL-13 receptor, STAT6 forms dimers, translocates to the nucleus and binds specific DNA sequences to regulate gene transcription (Fig. 4) (45, 47).

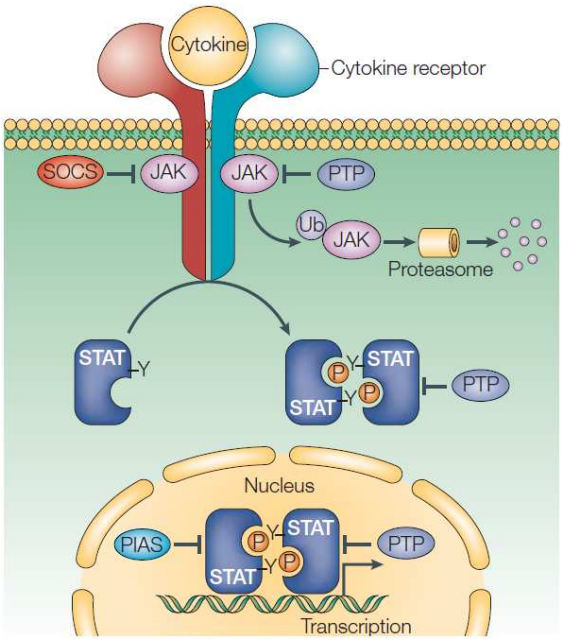

Figure 4. Schematic representation of the JAK-STAT pathway. Extracellular cytokines, i.e. IL-4 and IFN's interact with the transmembrane receptor and initiate an intracellular phosphorylation cascade mediated by receptor associated Janus kinases (JAK). JAKs phosphorylate tyrosine residues of cytoplasmic STAT, which dimerizes upon this modification. STAT homo- or heterodimers translocate to the nucleus and bind to canonical DNA elements. Nuclear co-activators induce transcription and chromatin modifications (45). Diagram reproduced from (46).

In a variation of the same theme, type I interferons, i.e. IFNγ, act as ligands by binding to the transmembrane receptor. Then, JAK1 and JAK2 phosphorylate cytoplasmic STAT1, which forms homodimers and is rapidly transported to the nucleus where it binds to the conserved DNA elements with the sequence of 5'-TT(N)$_{4-6}$AA-3'. In contrast, type II interferons (IFNα and IFNβ) lead to STAT1/STAT2 heterotrimers with the interferon regulatory factor 9 (IRF9). These heterotrimers, also called interferon-stimulated gene factor 3 (ISGF3), translocate to the nucleus and bind to the sequence 5'-AGTTT(N)$_3$TTTCC-3' (49).

The IFNγ induced IRF1 is an important target gene of STAT1 (50). As transcription factor, IRF1 regulates several gene clusters involved in host defense, cell proliferation and differentiation (51, 52). Therefore, IRF1 has an important role in innate immunity supplementary to its function as a tumor suppressor (53). Another target gene of IFNγ is ARTD9/BAL1 that was shown to be directly involved in the IFNγ signaling pathway (43).

The next level of complexity is added by the suppressor of cytokine signaling (SOCS) proteins, that are induced by cytokines (54). SOCS, Nmi, protein inhibitors of activated STATs (PIAS) and a STAT ubiquitin E3 ligase (SLIM) are negative regulators of the JAK-STAT pathway and act in a classical negative feedback loop (55–57). Together, they prevent the overreaction of the immune response.

1.3 Lymphoma

Originating from normal B-cells, malignant B-cells exploit intrinsic regulation mechanisms as cytokine signaling to usurp their host (58). These cancer cells acquire the ability to divide indefinitely, through accumulation of mutations in genes that are involved in cell growth and proliferation and epigenetic alterations (59). Their daughter cells inherit this characteristic to proliferate unrestrained, form a clone and subsequently a mass called tumor or neoplasm. A benign neoplasm remains localized and encased in a fibrous capsule; a malign tumor penetrates the basal lamina and spreads through the vascular system into the whole body. The daughter cells invade the tissue after re-attachment to the vascular endothelium, outgrow their environmental cells and form metastases. Primary neoplasm and metastases can remain asymptomatic or give rise to disease (1).

1.3.1 Subtypes of Lymphoma

White blood cell (WBC) neoplasms primarily arise from lymphocytes and are generally classified in leukemia and lymphoma. The former designates a lymphocytic cancer, which originates in the bone marrow and is generally manifest in the peripheral blood. The latter, in contrary, is usually of lymph node origin and forms a tumor mass most frequently in the lymph nodules itself. Dependent on the identification of Reed-Sternberg cells, the hallmark of Hodgkin disease, the lymphoma is classified in the two large categories Hodgkin and Non-Hodgkin lymphoma (NHL) (60). NHL has the highest incidence among lymphoid neoplasms in Switzerland as well as worldwide (61). Non-Hodgkin's B-cell lymphomas have characteristics of cancer, immunity and inflammation (62)

The most prevalent subtype of NHL, diffuse large B-cell lymphoma (DLBCL), accounts for 30–40% of new lymphoma cases per year (58). The histophathological features of this cancer are are large cell size and diffuse growth pattern and the cells stain positive for CD20.

DLBCL is considered an aggressive disease in humans (median age 60), although juveniles and children are affected too. If left untreated, this lymphoma is fatal after a short survival time. It is usually treated with an anthracycline based combination therapy consisting of **c**yclophosphamide, doxorubicin (**h**ydroxydaunorubicin), vincristin (**o**ncovin) and **p**rednisone (CHOP) (63). Recent progress due to the addition of anti-CD20 antibodies (Rituximab®) to CHOP (R-CHOP), led to remission rates between 60–80% (64). Notwithstanding this achievement, the survival rate stagnates, still 40–50% of the patients remain incurable and die of their disease (60).

Interestingly, DLBCL survival time, death risk and prognosis varies considerably among patients, albeit the histopathological properties are identical. This points to underlying molecular differences in DLBCL responsible for different outcome. Using molecular profiling, DLBCL was stratified in subgroups, which correlate with overall survival – germinal center B-cell (GCB)-like DL-

BCL has the longest survival after chemotherapy, activated B-cell (ABC)-like DLBCL the shortest (65, 66). Based upon these results, IL-4 was shown to sensitize GCB-like DLBCL to R-CHOP, while protecting ABC-like DLBCL from R-CHOP cytotoxicity (67). Since IL-4 levels in both GCB and ABC-like DLBCL are similar (68), this could be a reason for the different clinical outcomes.

1.4 Regulation of innate immunity and tumorigenesis through autophagy

Autophagy, from the Greek „$\alpha\upsilon\tau o\varsigma$" oneself and „$\phi\alpha\gamma\varepsilon\iota\nu$" to eat, denotes a catabolic cellular pathway that is conserved from yeast to mammals (69). There is mounting evidence that autophagic failure plays an important role in the pathogenesis of infectious diseases, cancer, myopathies, neurodegeneration, bone and metabolic disorders (70).

In cells, there exist two major degradation pathways: autophagy and the proteasome system. Proteins can be degraded by the 26S proteasome in a highly selective way. In contrast, lipids, intracellular proteins as well as whole organelles and pathogens can be targeted to the lysosomes for degradation. Autophagy evolutionarily emerged as a catabolic process to replenish the cell with nutrients during starvation (72). While different forms of autophagy have been described in mammalian cells, among them macroautopagy, microautophagy, piecemeal microautophagy of the nucleus and chaperone-mediated autophagy (CMA) (71), the following paragraphs will focus on macroautophagy, thereafter referred to as autophagy.

Autophagy is initiated when the phagophore, a membrane sac originating mainly from the endoplasmic reticulum (ER), grows and encloses cytoplasmic material to form the autophagosome (Fig. 5).

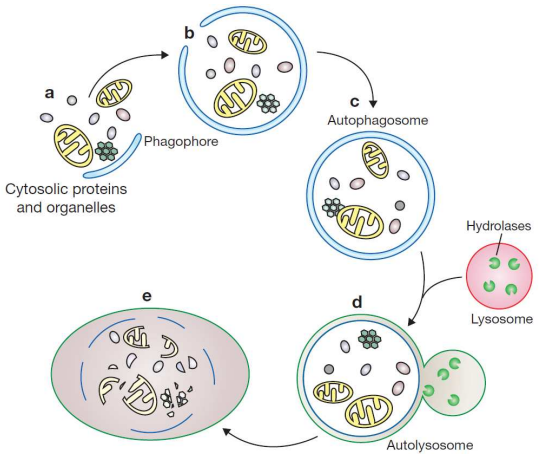

Figure 5. Schematic representation of autophagy. a,b,c. Cytoplasmic content is enveloped by the phagophore to form the autophagosome, a doubled membrane enclosing cytoplasmic content. d. The autophagosome fuses to a lysosome to form an autophagolysosome. e. Contents are then degraded together with the inner membrane. Diagram reproduced from (71).

Thereafter the autophagosome will fuse with a lysosome into an autophagolysosome. The contents of the autophagolysosome are then degraded by the lysosomal hydrolases and the resulting macromolecules (mostly amino acids) are used for further anabolic processes (71).

Even when nutrients are abundant, hepatocytes degrade 1-1.5% of their proteins per hour by autophagy (73). Quite reasonable, autophagosome formation is induced when cells are deprived of growth factors and nutrients such as amino acids (74–76). IFNγ, a pleiotropic cytokine, has also been found to induce autophagy in macrophages (77), T lymphocytes (78), mammary epithelial (79) and HeLa cells (80). In a negative feedback loop, restored amino acid levels re-establish basal levels of autophagy by activation of the serine/threonine protein kinase mammalian target of rapamycin complex 1 (mTORC1) (81). In this feedback loop, p62, a scaffold protein implicated in multiple cellular functions including autophagy, was found to interact with raptor, a component of the mTORC1 complex. p62 is required for amino acid sensing by mTORC1 (82). The absence of growth factors also inactivates mTORC1 in a phosphoinositide-3-OH kinase (PI3K) and phosphatase and tensin homolog on chromosome ten (PTEN) dependent way (83). mTORC1 is a major cell growth and proliferation regulator. Not surprising, it's activity is often deregulated in human cancer (84). For example, loss-of-function mutations in the gene of PTEN are detected at a rate almost as high as observed in tumor suppressor p53 (85, 86).

Downstream, mTORC1 phosphorylates eukaryotic initiation factor 4E-binding protein (4E-BP1) and 70kDa protein S6 kinase (p70S6K) to control protein synthesis. p70S6K phosphorylation is therefore often used as readout for the activity of mTORC1 (83).

1.4.1 Nucleation of the autophagosome

The molecular machinery of autophagy consists of 35 **au**to**p**ha**g**y-related (Atg) genes (88). It was studied in yeast, but many yeast genes have homologues in higher eukaryotes (89, 90). When nutrients are abundant, mTORC1 inhibits the unc-51-like kinase 1 (ULK1)/Atg1 complex consisting of the proteins ULK1, Atg13, FIP200, and Atg101 (Fig. 6).

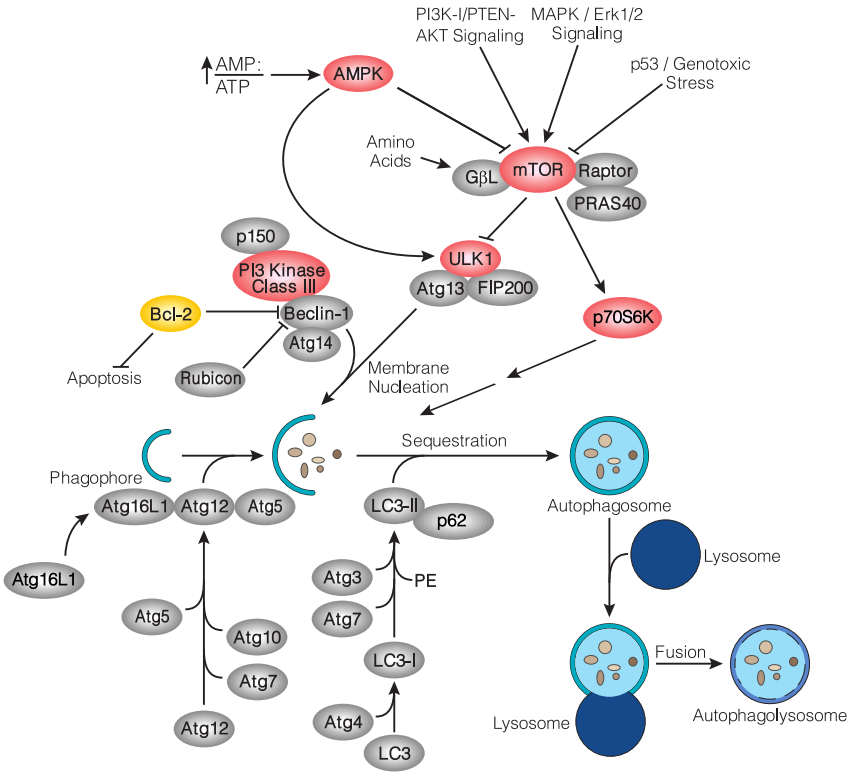

Figure 6. Schematic representation of the macroautophagy pathway. (Copyright © Cell Signaling Technology, Inc.), adapted from (87).

Upon starvation, autophagy is induced by the translocation of the ULK1 complex to the endoplasmic reticulum (ER). There, it interacts with the class III phosphatidylinositol-3-OH kinase complex (PIK3C3) (beclin 1, Atg14(L)/barkor, Vps15, Vps34, and ambra1) (83) which produces phosphatidylinositol-3-phosphate (PtdIns(3)P). PtdIns(3)P leads to the recruitment of double FYVE-containing protein 1 (DFCP1) and WD-repeat domain phosphoinositide-interacting (WIPI) family proteins to the autophagosome (6).

1.4.2 Elongation of the isolation membrane

Two ubiquitin-like conjugates are essential for the elongation and closure of the autophagosme-isolation membrane. First, the Atg7 (E1-like) and Atg10 (E2-like) enzymes conjugate Atg12 (ubiquitin-like) to Atg5. The Atg12–Atg5 conjugate forms thereafter a dimer together with ATG16L1 (91). Second, the Atg7 (E1-like) and Atg3 (E2-like) enzymes produce phosphatidylethanolamine (PE)-conjugated Atg8 homologues – Microtubule-associated protein light chain 3 (LC3), GATE16 and GABARAP – which are present on both sides of the isolation membrane (88, 92). The conversion of LC3 (LC3-I), which migrates with a molecular mass of 16kDa, to PE-conjugated LC3 (LC3-II), which runs faster on SDS-PAGE due to hydrophobicity (at approximately 14kDa), can be detected by western blot (93). At present, LC3-II is the best characterized marker for autophagy (94).

1.4.3 Selective autophagy

For a long time, (macro-)autophagy was considered a non-specific bulk degradation pathway. This view is not anymore appropriate, since p62/Sequestosome-1, a cargo receptor for selective autophagy, has been found (95, 96). p62 acts as platform to target proteins selectively to the autophagosome, together with the proteins neighbor of BRCA1 (NBR1) and nuclear dot protein 52 (NDP52) (69).

In chaperone-mediated autophagy (CMA), another well characterized selective autophagy pathway in mammalian cells, proteins containing the sequence KFERQ interact with the chaperone heat shock protein 70 (hsc70) to be degraded by the lysosome (97–100).

p62/Sequestosome-1

The protein p62/Sequestosome-1 is a substrate for selective autophagy but at the same time acts as adaptor for proteins degraded by selective autophagy. It mediates this function by physical interaction with all mammalian Atg8 analogs bound to the isolation membrane through its LC3-interacting region (LIR) (96, 101). When autophagy is inhibited, p62 accumulates and forms inclusion bodies together with ubiquitin (102). Such p62 positive protein aggregations have been identified in Alzheimer and Parkinson disease, amyotrophic lateral sclerosis, hepatitis, malignant glioma and hepatocellular carcinoma (103). p62-accumulation correlates negatively with the level of autophagic activity in cells, this is useful to monitor autophagic flux (94).

With its UBA domain, p62 binds to poly- and monoubiquitin *in vitro* (104–106). Mono-ubiquitinylation has been shown to be sufficient for substrates to be degraded by selective autophagy (107).

2 Aim

Despite the crucial, risk-related role of B aggressive lymphoma (BAL) proteins in DLBCL and their high evolutionary conservation, only few interaction partners of these proteins have been characterized to date. These include Signal transducer and activator of transcription (STAT) 6, p100 (TSN) and phosphoglucose isomerase (PGI)/autocrine motility factor (AMF) as interaction partners for ARTD8 and BBAP for ARTD9 (40, 108–110). According to own unpublished data ARTD8 interacts additionally with STAT2 and BBAP and ARTD9 forms complexes with STAT1, STAT2, IRF9 and BBAP (personal communication, P. O. Hassa). Identification of new binding partners could lead to a better understanding of the physiological role of BAL proteins in cancer and immunity.

The aim of this project was to investigate and functionally characterize binding partners of both the full length BAL proteins as well as their respective single and tandem *macro* domains using an unbiased approach. Several *macro* domain containing proteins are recruited to sites of nuclear ARTD1 activation induced by low power laser-generated DNA damage (36, 38, 111). Therefore, we set out to investigate whether the *macro* domains of BAL proteins interact with ARTD1 and other proteins.

For this purpose, we expressed His-GST tagged BAL *macro* domains in bacteria. After purification, these *macro* domains were used as bait in GST pull-downs with extracts of different mammalian cell lines. Then, the co-purified complexes were separated by SDS-PAGE and visualized using a silver stain. Subsequently the bands representing probable interaction partners were selected for identification by mass spectrometry. In a similar approach, hemagglutinin (HA) tagged full length ARTD9 protein was stably expressed in A549 cells, to investigate the interaction partners of the full length BAL proteins. Extracts from these cells were then used for co-immunoprecipitation experiments.

3 Materials and Methods

3.1 Solutions

3.1.1 Protein extraction buffers

WCE buffer
50 mM Tris pH 7.5
1% (v/v) NP-40
420 mM NaCl
Complete tablets (protease inhibitors) (Roche)
ddH_2O

Buffer A
50 mM Tris pH 7.5
Complete tablets (protease inhibitors) (Roche)
ddH_2O

Buffer A*
50 mM Tris pH 7.5
0.1% (v/v) NP-40
Complete tablets (protease inhibitors) (Roche)
ddH_2O

Buffer B
50 mM Tris pH 7.5
420 mM NaCl
1% (v/v) NP-40
Complete tablets (protease inhibitors) (Roche)
ddH_2O

3.1.2 SDS-PAGE and western blot solutions

5 x Running buffer
125 mM Tris base
1 M Glycine
0.5% Na-dodecylsulfate (SDS)
ddH_2O to 5 L

Solution B
1.5 M Tris pH 8.8
0.4% Na-dodecylsulfate (SDS)
ddH_2O

Solution C
0.5 M Tris pH 6.8
0.4% Na-dodecylsulfate (SDS)
small amount Bromphenol blue ddH_2O

10 x Transfer Buffer
25 mM Tris-base
192 mM Glycine
200 mL Methanol
ddH_2O to 1 L
Store at 4 ℃.

10 x TBS
100 mM Tris-HCl pH 7.5
1.5 M NaCl
ddH_2O to 1 L

TBST
100 mL 10 x TBS
0.5 mL Tween 20
ddH_2O to 1 L

10 x PBS
80 g NaCl
2 g KCl
14.4 g Na_2HPO_4
2.4 g KH_2PO_4
pH 6.8.
ddH_2O to 1 L

3.1.3 Silverstain solutions

According to a silver stain protocol from Ralph Imhof/Functional Genomics Center Zurich (FGCZ).

Fixing solution
50 % (v/v) EtOH
10 % (v/v) Glacial acetic acid
ddH_2O

Rinsing solution
50 % (v/v) EtOH
ddH_2O

Sensitizer, for 200 mL
0.058 g Sodium thiosulphate pentahydrate
ddH_2O

Stain, for 200 mL
0.2 g Silver nitrate
ddH_2O
Store on ice before use

Developer, for 500 mL
10 g Sodium carbonate
20 mL Sensitizer
200 μL Formaldehyde
ddH_2O

Stop solution
1 % (v/v) Acetic acid
ddH_2O

3.1.4 Bacterial medium

2 x LB medium, per 1 L Prepared according to (112).

Bactotrypton	20 g
Yeast extract	10 g
NaCl	10 g
ddH_2O to 1 L, autoclaved	

10 x PSB medium, per 1 L Prepared according to Paul O. Hassa, personal communication.

Bactotrypton	100 g
Yeast extract	20 g
Casamino acids	20 g
NaCl	50 g
NH_4Cl	10 g
KH_2PO_4	30 g
Na_2HPO_4	60 g
ddH_2O to 1 L	
pH adjusted to 7.2, autoclaved.	

3.1.5 Antibodies

Anti-phospho-AMPK (Thr172)	Rabbit monoclonal 40H9, Cell Signaling, #2535, used at 1:1000
Anti-AMPKα	Cell Signaling, #2532, used at 1:1000
Anti-ARTD1	Immunization done at UZH, used at 1:2000
Anti-ARTD8	Gift from A. Raz (110), used at 1:1000
Anti-ARTD9	Millipore, C-terminal, AB10618, used at 1:250
Anti-ARTD10	Aviva Systems Biology, ARP42810_P050 and ARP42811_P050, used at 1:1000
Anti-ARTD13	GeneTex, GTX120134, used at 1:20,000
Anti-beclin-1	Santa Cruz Biotechnology, used at 1:1000
Anti-HA	Sigma, monoclonal HA-7, used at 1:10,000
Anti-LC3A/B	Cell Signaling, #4108, used at 1:1000
Anti-Nucleolin	Santa Cruz, sc-8031, used at 1:1000
Anti-Nucleolin	GeneTex (for mouse), GTX16940, used at 1:1000
Anti-p62	Epitomics, 3340-1, used at 1:10,000
Anti-p68	Millipore, clone PAb204, used at 1:1000
Anti-phospho-p70S6K (Thr389)	Cell Signaling, #9205, used at 1:1000
Anti-PAR	10H from (113), used at 1:5000
Anti-PAR	Becton Dickinson, LP-96-10, used at 1:3000
Anti-Tubulin	Sigma, used at 1:10,000
Secondary Antibodies	
Anti-rabbit	ECL TM anti-rabbit IgG, horseradish peroxidase linked whole antibody (from donky), NA934V, GE Healthcare UK Limited
Anti-mouse	ECL TM anti-mouse IgG, horseradish peroxidase linked whole antibody (from sheep), NA931V, GE Healthcare UK Limited

3.2 Bacterial protein expression

3.2.1 Plasmids and sequencing

pETM33 vectors (P. O. Hassa & EMBL core facility) were used for the cloning and expression of $(His)_6$-GST tagged single and tandem (duplicated) *macro* domains. Cloning was performed by Paul O. Hassa. Sequencing of plasmids was performed by Microsynth (Balgach). Minipreps and preparation of chemically competent cells were performed according to standard methods (112).

3.2.2 Expression of $(His)_6$-GST tagged *macro* domains in bacteria

50μL competent BL21(DE3) pLysS cells (Novagen) were thawed on ice for 10 min, transformed with 5μL plasmid DNA by heatshock at 42°C for 50 s and incubated again 2 min on ice. Then, the *E. coli* cells were incubated with 400μL Luria Bertani (LB) medium without antibiotics for 1 h at 37°C. The whole suspension was added to 15 mL LB medium with 50μg/mL chloramphenicol and 50μg/mL kanamycin and incubated over night at 37°C.

ARTD7, ARTD8 and ARTD9 single and tandem *macro* domains were expressed in 200 mL PSB medium supplemented with 50μg/mL chloramphenicol and 50μg/mL kanamycin as $(His)_6$-GST fusions at 16°C for 16 h with 200 μM IPTG induction. The culture suspension was centrifuged for 20 min at 4000 rpm (5299 rcf) in a H6000A rotor (Sorvall 3C centrifuge, Fisher Scientific) to harvest the bacteria. The resulting pellets were resuspended in ice-cold resuspension buffer (50 mM Tris-HCl, pH 7.5, 500 mM NaCl, 10% glycerol, 2 mM PMSF) by shaking at 260 rpm, 0°C, snap-frozen in liquid N_2 and stored at −80°C.

3.2.3 Nickel purification of $(His)_6$-GST tagged *macro* domains

Cell suspension was thawed in a cold water bath, supplemented with lysozyme, 1% NP-40 and 2 mM PMSF and lysed rotating at 4°C for 1 h. DNAse I and 10 mM $MgCl_2$ were added to digest nucleic acids and the suspension was rotated for an additional hour at 4°C. The lysate was centrifuged for 30 min at 12000 rpm (17600 rcf) in a SS-34 rotor at 4°C (Sorvall RC 5C PLUS centrifuge, Fisher Scientific). The supernatant "crude protein extract" was incubated for 2 h with High Performance Nickel Sepharose (Amersham Biosciences, Sweden), after adjustment of the NaCl concentration to 1 M. Beads were washed twice with 15 mL of washing buffer (50 mM Tris-HCl, pH 7.5, 1 M NaCl, 0.5% NP-40 and 2 mM PMSF) and once with the same buffer containing 1.5 M NaCl. Elution was done with elution buffer containing 50 mM Tris-HCl pH 8, 200 mM imidazole and 100 mM NaCl. After addition of 10% glycerol, the purified proteins were snap-frozen in liquid N_2 and stored at −80°C.

3.3 Mammalian cell culture

3.3.1 Cell lines and culture conditions

All media were stored at 4℃ and preheated to 37℃ in a warm water bath before use. Mammalian cells were cultured at 37℃ and 5% CO_2, in a humified incubator. Cell culture experiments were performed under a sterile hood. A modified Neubauer counting chamber was used to determine the exact cell number.

293T

The Human embryonic kidney cell line (293T) is a derivative of the human primary embryonal kidney cell line 293 additionally containing the SV-40 large T-antigen. These cells are easily transfectable by the calcium phosphate method. 293T cells were cultured in Dulbecco's modified Eagle's medium (DMEM) substituted with 10% Fetal bovine serum (FBS), 2 nM L-glutamine and addition of (50 U/mL) penicillin and (50 μg/mL) streptomycin. Cells doubled approximately every 24 hours and were split 1:10 when they reached 90% confluence (every three days).

RAW-264.7

This line of mouse monocytes/macrophages was originally isolated from a mouse tumor induced by a Abselon leukaemia virus. Adherent Mouse monocyte/macrophage cell line (RAW-264.7) macrophages were grown in RPMI-1640 medium supplemented with 10% FBS and penicillin (50 U/mL)/ streptomycin (50 μg/mL). Cells doubled approximately every 24 hours and were split by scraping 1:3 when they reached 90% confluence.

A549

The A549 cell line was established in 1972 by D. J. Giard, et al. through the removal and culturing of cancerous lung tissue in the explanted tumor a of 58-year-old caucausian male. A549 cells are immortalized human type II bronchial epithelial cells obtained from lung carcinomatous tissue. The adherent cells were cultured in DMEM substituted with 10% FBS, 2 nM L-glutamine and addition of (50 U/mL) penicillin and (50 μg/mL) streptomycin. Cells doubled approximately every 24 hours and were split 1:10 when they reached 90% confluence (every three days). The stable cell lines A549 empty and A549 HA-ARTD9 were established by co-transfection of A549 cells with the PiggyBac plasmid containing no insert or the cDNA for HA tagged human ARTD9/BAL1 isoform 2 together with a recombinase plasmid with Lipofectamine 2000 (Invitrogen). Cloning of the PiggyBac plasmids was performed by Paul O. Hassa.

U-2932

The human B-cell line U-2932 was derived from ascites of a DLBCL patient previously treated multiple times for Hodgkin lymphoma (114). It is Eppstein-Barr virus negative. The suspension cells were cultured in RPMI-1640 medium supplemented with 10% FBS and antibiotics (penicillin 100 U/mL/streptomycin 50 μg/mL). Cells doubled approximately every 48 hours and were split 1:3 when they reached 90% confluence.

3.3.2 Preparation of whole cell extracts (WCE)

After aspiration of the supernatant, adherent cells were washed with 10 mL PBS and harvested with 4 mL PBS EDTA per 10 cm dish. Suspension cells were directly transferred to a 50 mL tube (TRP) and semi-adherent macrophages (RAW-264.7) and SU-DHL-7 lymphocytes were scraped. An aliquot of the cell suspension was taken for a subsequent western blot. Then, the cell suspension was centrifuged for 3 min at 1000 rpm, the supernatant was aspirated and cell pellets were frozen and stored at −80℃. After thawing, 3 pellet volumes of WCE buffer were added to the pellets. After pipetting up and down, transfer to an Eppendorf tube and vortexing of the solution, the solution was rotated for 30 min at 4 ℃. Non soluble cell debris was removed by centrifugation at 14000 rpm for 30 min at 4 ℃. The remaining supernatant was called whole cell extract (WCE).

3.3.3 Preparation of cytoplasmic and nuclear extracts

After aspiration of the supernatant, adherent cells were washed with 10 mL PBS and harvested with 4 mL PBS EDTA (1.5 mM) per 10 cm dish. Suspension cells were directly transferred to a 50 mL tube (TRP) and semi-adherent macrophages (RAW-264.7) were scraped. An aliquot of the cell suspension was taken for a subsequent western blot. Then, the cell suspension was centrifuged for 3 min at 1000 rpm, the supernatant was aspirated and cell pellets were frozen and stored at −80℃. After thawing, 3 pellet volumes of buffer A were added to the pellets. After 5 min equilibration, the suspension was centrifuged at 5000 rpm and 4 ℃ for 5 min. The resulting pellet was resuspended in the 3 pellet volumes buffer A*, incubated for 1–3 min, and centrifuged again at 5000 rpm and 4 ℃ for 10 min. The supernatant "cytoplasmic extract" was pipetted in new Eppendorf tubes. After resuspension of the pellet in buffer B, the solution was rolled for 30 min at 4 ℃. Non soluble cell debris was removed by centrifugation at 14000 rpm for 30 min at 4 ℃. The remaining supernatant was termed nuclear extract.

3.3.4 H_2O_2 treatment of U-2932 cells

U-2932 cell suspension was centrifuged for 3 min at 1000 rpm and supernatant was aspirated. Then the pellet was resuspended with serum free medium or PBS containing 1 mM H_2O_2 and cells were

incubated for 10 min at room temperature. Thereafter, cells were centrifuged again for 3 min at 1000 rpm, the supernatant was aspirated and the cell pellets were frozen and stored at −80℃.

3.3.5 Endotoxin stimulation

E. coli lipopolysaccharide (LPS) from Escherichia coli 055:B5 (Sigma, L2880) was directly added to the cell culture medium for stimulation at a final concentration of 100ng/mL. The cells were stimulated for 4 h and then harvested as described in paragraph 3.3.2.

3.3.6 Serum starvation

Cells grown in 6-well plates were treated when they reached 70-90% confluency. Firstly, the cells were washed twice with 2 mL DMEM without FCS. Then 3 mL DMEM without FCS was added to the cells for the time indicated.

3.3.7 siRNA mediated gene knockdown

The transient knockdown of beclin-1 and p62 in A549 empty and BAL1 cells was carried out as follows:

Day 0 Reverse transfection: 500μL OptiMem (Invitrogen) medium, 2μL of a 20 nM siRNA stock (siCTR or siBecn-1, Ambion) and 4μL Lipofectamine RNAiMax (Invitrogen) were premixed and incubated at RT for 20 min. A549 empty and BAL1 cells were seeded at a density of 5x10^5 cells per well of a 6-well plate, mixed with the transfection mix and allowd to adhere overnight.

Day 1 The medium was changed in the morning.

Day 2 or 3 The cells were harvested as described in paragraph 3.3.2 to control the success of the knockdown by western blot using an antibody specific for beclin-1 or p62. Alternatively, the cells were first treated with serum starvation to induce autophagy as described in paragraph 3.3.6 and harvested subsequently.

The beclin-1 siRNA was a gift from C. Blenn, Institute of Pharmacology, Zurich. p62 siRNA was synthesized by Quiagen according to the sequence p62-2 published in (115).

3.4 Interaction studies

3.4.1 GST pull-down assay

GST pull-down assays were performed according to manufacturers procedure (Amersham/GE) with Glutathione-Sepharose 4B affinity beads, and as described in the figure legends. Briefly, His purified $(His)_6$-GST tagged *macro* domains were rebound for 2 h with 10-20 μL Glutathione-Sepharose (Amersham Biosciences, Sweden) in 1 mL BB (50 mM Tris pH 7.5, 1% NP-40 and 250 mM NaCl) at 4℃. Then the beads were washed 2x with WB1 (50 mM Tris pH 7.5, 1% NP-40 and 250 mM NaCl) and WCE as decribed in 3.3.2 were prepared and incubated for 2 h with the beads, after adjustment of the NaCl concentration to 100 mM. To reduce false positive interaction partners, ethidium bromide (EtBr) at a concentration of 50μg/ml was added to the WCE before performing the pull-down assay. After 3 washing steps with WB2 (50 mM Tris pH 7.5, 0.2% NP-40 and 100 mM NaCl), the proteins were eluted with 60 μL 2x LB at 95℃ for 3 min and separated by SDS-PAGE as described in 3.5.1.

3.4.2 Hemagglutinin-Co-Immunoprecipitation

Hemagglutinin-Immunoprecipitation (HA-IP) were performed as previously described (116). Briefly, 10-20 μL HA-Agarose (Sigma, clone HA-7) were washed 2x with WB1 (50 mM Tris pH 7.5, 1% NP-40 and 250 mM NaCl). Whole cell extracts (WCE) as decribed in 3.3.2 were prepared and incubated with the beads for 2 h. After 3 washing steps with WB2 (50 mM Tris pH 7.5, 0.2% NP-40 and 100 mM NaCl), the proteins were eluted with 60 μL 2x LB at 95℃ for 3 min and separated by SDS-PAGE as described in 3.5.1.

3.5 Detection methods

3.5.1 SDS-PAGE

To separate a protein mixture according to their molecular weight, SDS-PAGE was performed. At first, glass plates were cleaned with Ethanol (EtOH) and dddH_{20}. Then a 10% separating gel was cast using 1/4 (v/v) acrylamide (acrylamide-bis solution 37.5:1, 40% (w/v), SERVA Electrophoresis), 1/4 (v/v) solution B and ddH_{20} to the final amount. 1/100 (v/v) APS (10%) and 1/1000 (v/v) TEMED were used to let the gel polymerize. On top of the separating gel, a 4% stacking gel was cast and a comb to create the sample pockets was inserted before polymerization. Before usage, sample pockets were rinsed with running buffer to remove not polymerized acrylamide. Samples were loaded into pockets and one lane was used to load a marker of distinct molecular weights. The electrophoresis unit was filled with running buffer and run at 90–125V for an hour. When

the bromphenol blue line reached the lower edge of the gel, the electrophoresis apparatus was disconnected, disassembled and the gel was either stained (as described in paragraphs 3.5.2, 3.5.3) or immunoblotted (described in paragraph 3.5.4).

3.5.2 Silverstain

The whole staining procedure was performed on a lab shaker at 100–200 rpm. The polyacrylamide gel was washed for 30 min in ddH_2O and fixed for 10 min in fixing solution. Thereafter, the gel was incubated for 5 min in rinse solution and sensitized for 2 min. After a short 2 min wash in ddH_2O, the gel was stained for 20 min, washed twice for 1 min and developed for a maximum of 10 min. The developer was changed after one minute. Staining was stopped by incubation for at least 5 min in stop solution, thereafter, the PAGEs were washed three times with ddH_2O.

3.5.3 Roti®-Blue

This sensitive colloidal coomassie G-250 staining solution with a low detection limit was prepared according to manufacturer's instructions (Roth). It's based on a protocol described in (117). The gels were incubated over night in a closed container and destained afterwards with ddH_2O. Indicated bands were cut out, transferred to Eppendorf tubes and stored at -20℃ until tandem mass spectrometry was performed 3.5.6.

3.5.4 Western blot

Resolved proteins were transfered from the polyacrylamide gel onto a methanol activated PVDF membrane (Immobilon-FL, Millipore) at a current of 100V for 1h or alternatively at 30 V over night. After 1 h incubation in blocking solution 10% milk (Migros) in TBST) to avoid unspecific binding, the membrane was incubated for 2 h with the primary antibody diluted in TBST and 0.5% milk. Afterwards the membrane was washed 3 x with TBST and incubated for 1 h with the appropriate secondary antibody. The membrane was washed again 3 x with TBST, drained and developped with enhanced chemiluminescence (ECL) solution (Fisher Scientific) and exposed to X-ray film (Raymed Imaging, Typox TX-RP) for 1 s–15 min. Phosphorylated proteins and LC3B were detected by using phosphorylation specific antibodies and the substrate SuperSignal West Femto (Fisher Scientific), an ultra sensitive ECL solution. To minimize background, the membranes were blocked for 1h at RT in 5% milk (Migros)/3% bovine serum albumin (Sigma) in TBST) and washed with TBST containing 2.5% milk (Migros) after each incubation with antibodies. Before developing with the ECL substrate, the membrane was again 3 x washed with TBST (without milk).

3.5.5 Quantitative PCR

Total RNA from cells was isolated using TriReagent (Luzerna). Cells were washed with PBS and 0.5 mL and TriReagent was added directly to a 6-well to resuspend cells by up and down pipetting. The cell suspension was transfered to an Eppendorf tube, 0.1 mL chloroform was added and the tube was vortexed for 15 s. The suspension was incubated at room temperature until it was well separated and then centrifuged at 12000 g for 15 min at 4℃. The aqueous phase containing the RNA was transferred to a new Eppendorf tube and mixed with 0.25 mL isopropanol. After a centrifugation step (12000 g, 10 min, 4℃), the pellet was washed with 0.5 mL 75% ethanol by vortexing and centrifuged again (7500 g, 10 min, 4℃). Thereafter the RNA was air dried and dissolved in 10 mM Tris (pH 7.5). The RNA was subsequently reverse-transcribed using the 'High-capacity cDNA reverse transcription kit' (Applied Biosystems). Real-time qPCR was performed using the Rotor-Gene 3000 (Corbett Life Science) and SYBR Green according manufacturers protocols. Primers used for ARTD9 FWD GGCAAAGAGGTCCAAGATGCTG and REV GCCTCACACATCTCTTCCACGT and GAPDH FWD GAAATCCCATCACCATCTTCC and REV GAGCCCCAGCCTTCTCCATG. Values were calculated according to the $2^{-\Delta Ct}$ method and normalized to GAPDH mRNA. Mean and standard deviation was calculated.

3.5.6 Tandem mass spectrometry

Liquid chromatography/electrospray ionisation/mass spectrometry/mass spectrometry (LC/ESI/MS/MS) was carried out by the Functional Genomics Centre Zurich as follows.

Gel bands were cut in small pieces and washed 2 x with 100 μL 100 mM NH_4HCO_3/50% acetonitrile and again washed 1 x with 50 μL acetonitrile. All three supernatants were discarded. Digestion was carried out by addition of 10 μL trypsin (10 ng/μl in 10 mM Tris/2 mM $CaCl_2$, pH 8.2) together with 20 μL buffer (10 mM Tris/2 mM $CaCl_2$, pH 8.2) at 37° C over night. Supernatant was removed and gel pieces were extracted 2 x with 100 μL 0.1% TFA/50% acetonitrile. All three supernatants were combined and dried. Samples were dissolved in 25 μL 0.1% formic acid and transferred to autosampler vials for LC/MS/MS. 4 μL (9 μl for band 93 and 95) were injected.

Database searches were performed by using the ProteinLynx Global Server (SwissProt, all species) and Mascot (NCBI_nr, all species; SwissProt, all species) search programs. Only Mascot results are shown (PLGS results were essentially the same). Mascot results were summarized in Scaffold (trypsin, keratins and bait proteins were hidden).

Database searching

Charge state deconvolution and deisotoping were not performed. All MS/MS samples were analyzed using Mascot (Matrix Science, London, UK; version Mascot). Mascot was set up to search

the fgcz_swissprot_20110111 database (unknown version, 524680 entries) assuming the digestion enzyme trypsin. Mascot was searched with a fragment ion mass tolerance of 0.050 Da and a parent ion tolerance of 10.0 PPM. Oxidation of methionine and acrylamide adduct of cysteine were specified in Mascot as variable modifications.

Criteria for protein identification

Scaffold (version 3.3.2, Proteome Software Inc., Portland, OR) was used to validate MS/MS based peptide and protein identifications. Peptide identifications were accepted if they could be established at greater than 95.0% probability as specified by the Peptide Prophet algorithm (Keller, A et al Anal. Chem. 2002;74(20):5383-92) (118). Protein identifications were accepted if they could be established at greater than 95.0% probability and contained at least 1 identified peptides. Protein probabilities were assigned by the Protein Prophet algorithm (, AI Anal Chem. 2003 Sep 1;75(17):4646-58) (119). Proteins that contained similar peptides and could not be differentiated based on MS/MS analysis alone were grouped to satisfy the principles of parsimony.

3.6 *In silico* methods and software

3.6.1 Multiple sequence alignments

A multiple sequence alignment (MSA) of ARTD7-9, mH2A1.1, mD1, mD2, C6orf130, Af1521 and SARS nsp3 was made using the M-Coffee web server (120–122). The MSA was refined using ClustalX 2.1.

3.6.2 Domain structure prediction

BAL1/ARTD9 (NP_001139574.1, 854aa, human PARP9 isoform a), BAL2/ARTD8(NP_001034619.2, 1817aa, mouse PARP14) and BAL3/ARTD7(NP_001106995.1, 678 aa, human PARP15 isoform 1) FL sequences were queried against InterPro (available online: `http://www.ebi.ac.uk/Tools/pfa/iprscan/`) and domain borders were manually validated with Phyre (available online: `http://www.sbg.bio.ic.ac.uk/~phyre/`) (123).

3.6.3 Protein structure prediction and modeling

I-TASSER (available online: `http://zhanglab.ccmb.med.umich.edu/I-TASSER/`) (124) was used to predict the structure of BAL1/ARTD9 (NP_001139574.1, 854aa, human PARP9 isoform a), BAL2/ARTD8(NP_001034619.2, 1817aa, mouse PARP14) and BAL3/ARTD7(NP_001106995.1, 678

aa, human PARP15 isoform 1) FL proteins . Subsequently, protein structures were modeled using PyMOL 1.2r1 software (125).

3.6.4 Software

ClustalX 2.1 (multiple sequence alignments)
Scaffold 3.2.2 (analysis of mass spectrometry data)
PyMOL 1.2r1 (125) (structure modeling)
Inkscape 0.47 (vectors)
Gimp 2.6 (graphics)
XeTeX and BibTeX (desktop publishing and literature database)
LibreOffice (simple statistics)

4 Results

4.1 Identification of *macro* domain specific interaction partners

Only few protein-to-protein interaction partners of BAL proteins are characterized to date (for details see introduction). To identify further *macro* domain specific interaction partners, a GST pull-down approach with subsequent mass spectrometry analysis was established as shown in Fig. 1.

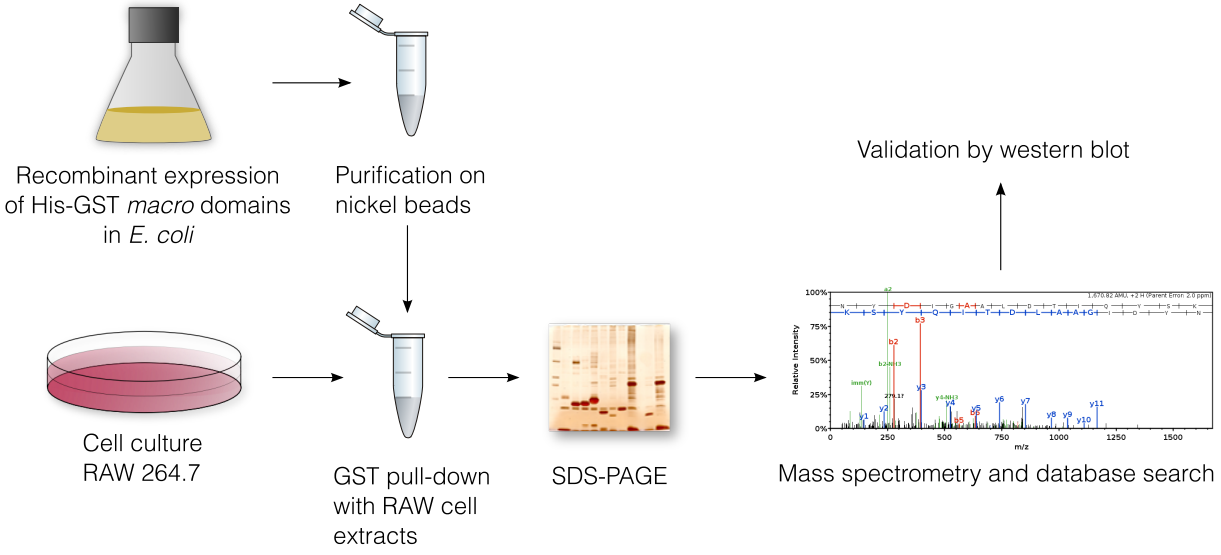

Figure 1. Schematic representation of the established GST pull-down setup to identify further interaction partners of BAL proteins.

At the beginning, single and tandem *macro* domains cloned into the pETM33 vector were recombinantly expressed as His-GST fusions in bacteria. Then GST pull-downs were performed with mammalian cell extracts and the co-purified proteins were separated by SDS-PAGE according to molecular weight. The polyacrylamide gels were analyzed after silver staining and specific bands were cut and sent to mass spectrometry for identification. The identified proteins were then validated by further GST pull-downs and HA-immunoprecipitations analyzed by western blot.

4.1.1 Multiple sequence alignment

A multiple sequence alignment (MSA) of ARTD7-9, mH2A1.1, mD1, mD2, C6orf130, Af1521 and SARS nsp3 was made using the M-Coffee web server (120–122). M-Coffee is a meta-server that combines several multiple sequence alignment algorithms and using this strategy outperforms other methods for MSA. Conserved blocks and differences between the protein sequences of the different *macro* domains are shown in Fig. 2.

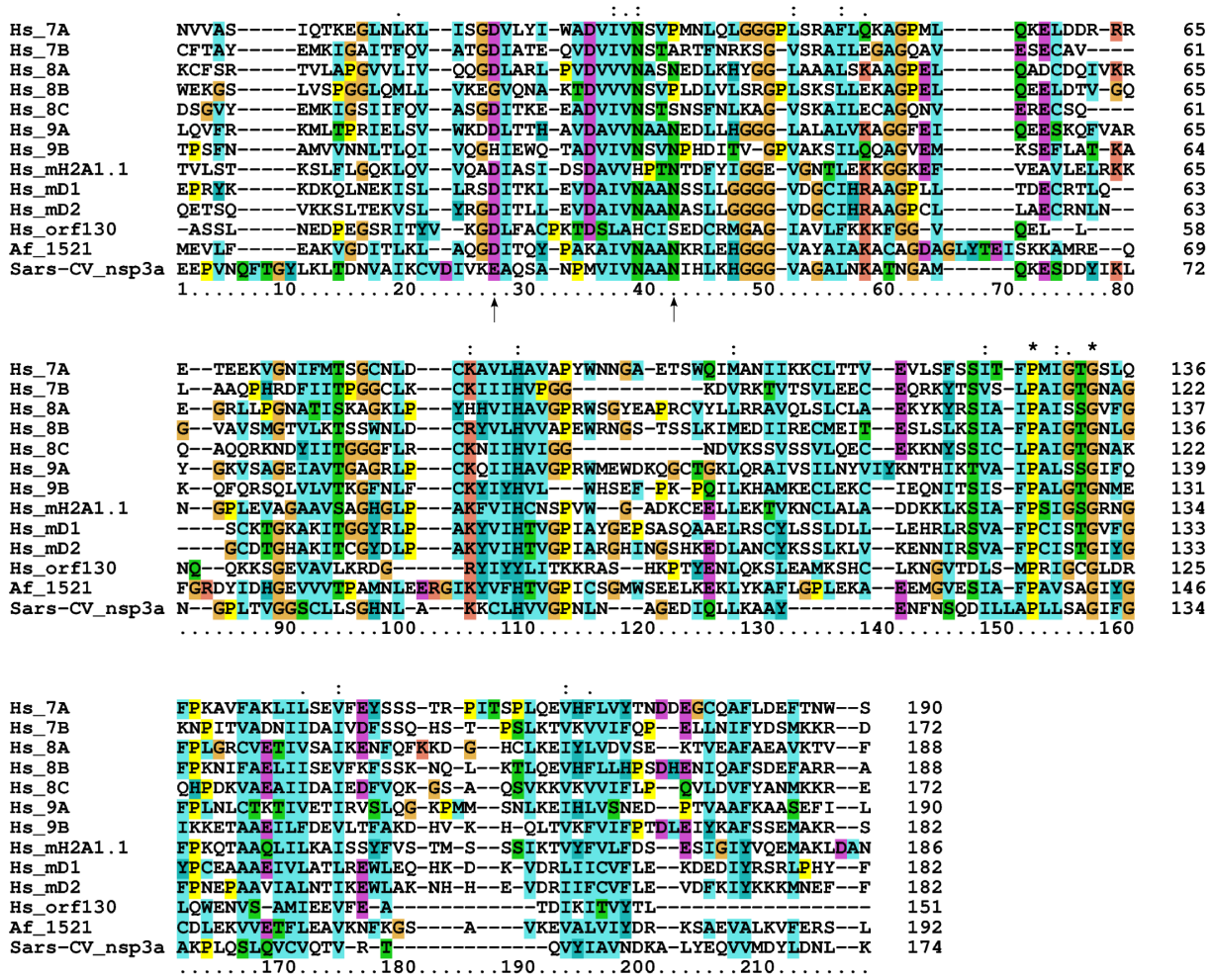

Figure 2. Multiple sequence alignment of different *macro* domains. *Macro* domain sequences of ARTD7-9, mH2A1.1, mD1, mD2, C6orf130, Af1521 and SARS nsp3 were aligned using M-Coffee. Above the alignment column conservation is indicated. Identical residues are marked with an asterisk, highly conserved residues with a colon (:). Residues important for ADPr binding in Af1521 are indicated with arrows. Single *macro* domains of ARTD7–9 are referred to as 7B, 8C, 9B.

A first overview reveals that the sequence of *macro* domains of viral, bacterial and human origin is highly conserved. Specific binding properties for the different *macro* domains are inferred, since the aspartic acid (D20) and asparagine (N34), that were found to be important for ADPr binding by Af1521 (33) (indicated with arrows in Fig. 2), are not conserved in *macro* domains 7A/B, 8B/C and

9B. In contrast, these residues are conserved in the *macro* domains mH2A1.1 and mD2. The latter two *macro* domains are therefore proposed to bind ADPr, while the former could have altered binding properties.

4.1.2 Structure modeling

So far, only single domain structures of the BAL proteins are solved by X-ray crystallography. I-TASSER (available online: `http://zhanglab.ccmb.med.umich.edu/I-TASSER/`) is one of the most accurate public protein structure prediction servers as assessed by CASP7, 8 and 9 experiments (124). To assess if the different binding patterns of the BAL proteins (cf. Fig. 2) and their respective *macro* domains could be explained by their structure and to get an impression of the overall BAL proteins, their structure was modeled with I-TASSER and viewed in PyMOL.

Estimated Tm-score and root-mean-square-deviation (RMSD) are measures of similarity of the predicted models and are used to compare the structure of a predicted model relative to its native state. Tm-score weighs the core matches stronger and is therefore more sensitive. ARTD7 was modeled with an estimated accuracy of 0.30±0.10 TM-score and 18.1±2.4 Å RMSD. As assessed by estimated Tm-score and the amount of coils to the number of sheets and helices predicted, this models is only appropriate to give a rough structural overview. Since ARTD8 was modeled with an estimated accuracy of 0.53±0.15 TM-score and 13.7±4.0Å RMSD and the estimated accuracy for ARTD9 was 0.51±0.15 TM-score and 12.6±4.3Å RMSD, these two models are expected to be in the right fold (126). Stereo ribbon representations of the models are shown in Fig. 3.

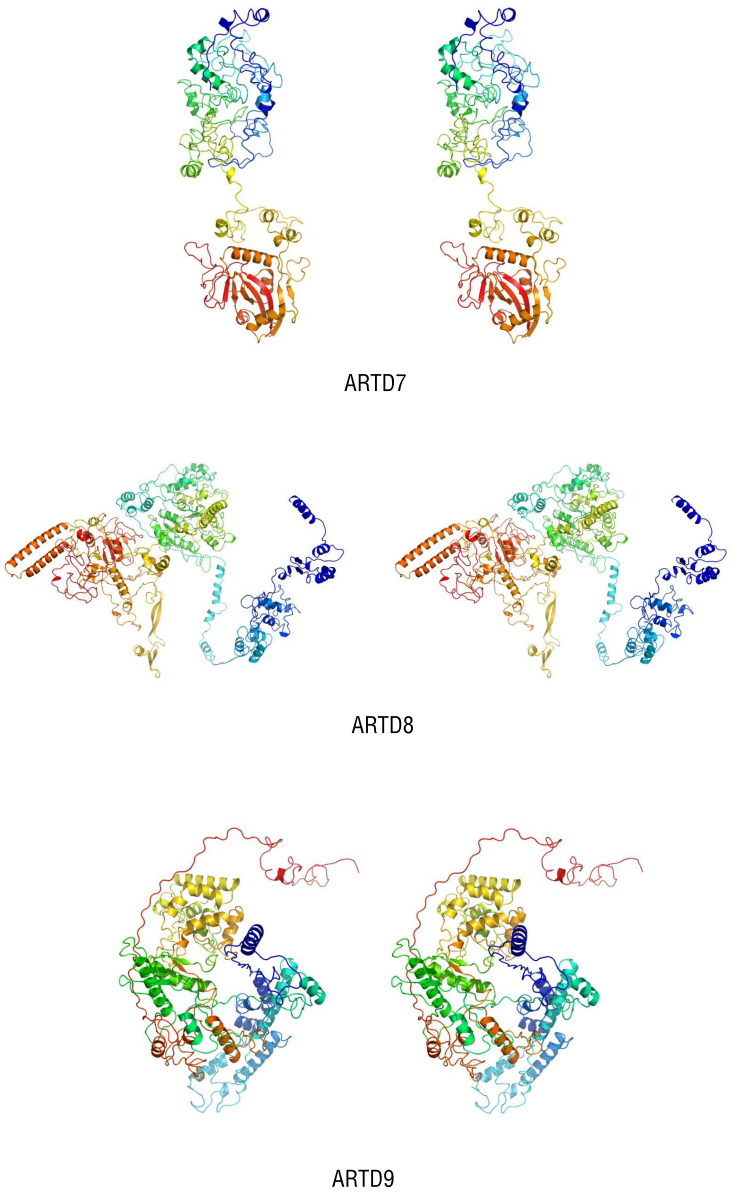

Figure 3. Stereo ribbon representation of the ARTD7-9 overall structure colored in a blue-to-red gradient (from amino-terminus to carboxy-terminus). The figures were prepared using the software PyMOL (125).

4.1.3 Expression of *macro* domains in bacteria

AF1521 wildtype (WT) and mH2A1.1 WT were intended as PAR and ARTD1 binding positive controls, GST, AF1521 binding mutant (mut) and mH2A1.1 mut as negative controls. The *macro* domain of *macro* D2, a mammalian protein of unknown function, was previously shown to bind monomeric ADPr with high affinity (Kd = 0.15 μM). However, it did not bind PAR efficiently (29). Thus, we chose it as mono-ADP-ribose binding control. Single *macro* domains of ARTD7–9 are referred to as 7B, 8C, 9B. The two *macro* domains of ARTD9 expressed in tandem are termed 9Tm.

After purification on nickel beads, proteins were separated by 10% SDS-PAGE and stained with Comassie as shown in Fig. 4.

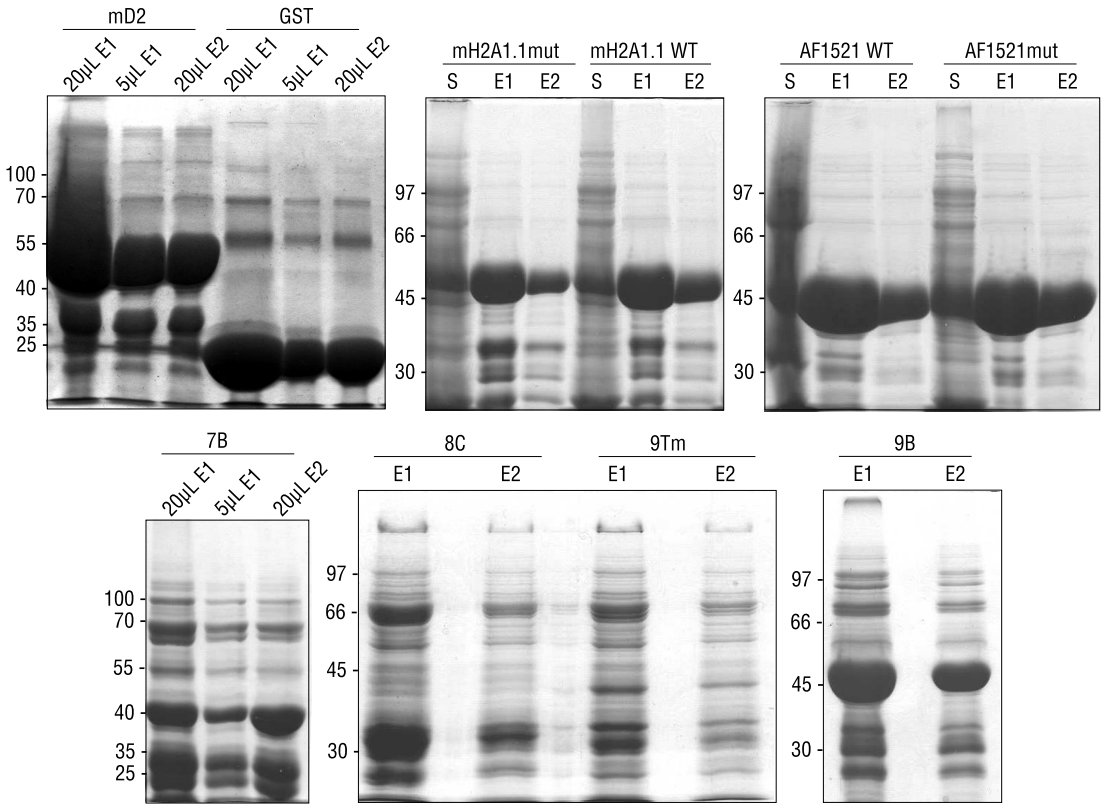

Figure 4. Expressed macrodomains were purified on high performance nickel sepharose, separated by 10% SDS-PAGE and stained with Coomassie blue. E1 and E2 indicate Elution 1 and Elution 2 respectively. The estimated molecular weight for His-GST-9Tm is ∼75 kD.

For the following GST pull-down experiments, the nickel purified His-GST fusion proteins were rebound to glutathione sepharose. Then the beads were washed before mammalian cell extracts were added to remove contaminating bacterial proteins. By this tandem affinity purification a high purity of the fusion proteins was achieved (Fig. 5 and 9).

4.1.4 Optimization of NaCl concentration for GST pull-downs

To use a NaCl concentration for GST pull-downs that stabilizes specific and reduces unspecific binding, salt concentration dependent interactions were analyzed for AF1521 WT and its binding mutant (AF1521 mut) as well as for mH2A1.1 WT and mH2A1.1 mut.

GST was used as negative control. This pull-down was performed with untreated nuclear extract from 293T cells. After boiling the beads in SDS Lämmli buffer for 3 min at 100°C, co-purified proteins were separated by SDS-PAGE and analyzed by silver staining (Fig. 5).

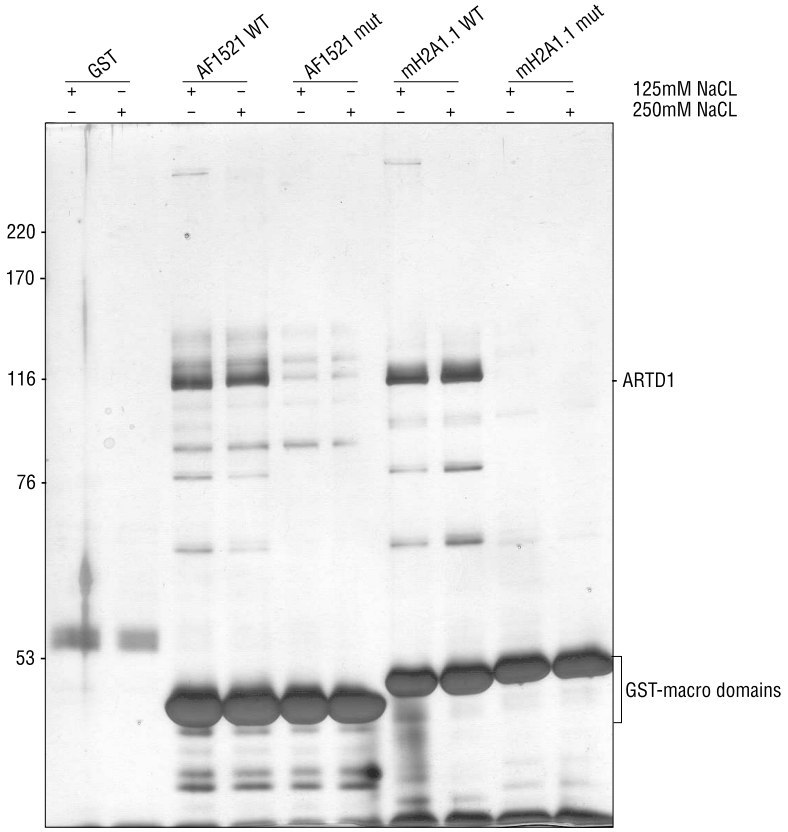

Figure 5. Optimization of NaCl concentration for GST pull-downs. Nuclear 293T extracts were bound at 125/250mM NaCl concentration to immobilized *macro* domains. 7.5% SDS-PAGE silver stained. ARTD1 indicates the size of the band identified by western blot (6) as ARTD1.

The following GST pull-downs were performed at a NaCl concentration of 210mM, according to the results of this optimization experiment. Of note is the high purity achieved after rebinding of the nickel purified *macro* domain proteins to glutathione sepharose, as analyzed by silver staining.

4.1.5 ARTD1 from untreated 293T extracts binds to mH2A1.1 and AF1521 macro domains

The interaction of ARTD1 with positive control *macro* domains was analyzed by western blot to identify ARTD1 (Fig. 6).

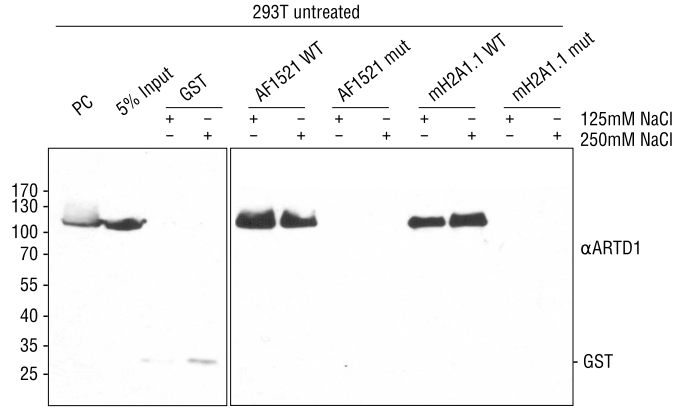

Figure 6. The same GST pull-down as in Fig. 5 analyzed by western blot against ARTD1. AF1521 WT and mH2A1.1 WT bind ARTD1 at 125 and 250mM NaCl concentration. An untreated 293T extract was used as positive control (PC).

As previously published, AF1521 WT and mH2A1.1 WT bind ARTD1 and can therefore be used as positive controls (33, 35). To prove this protein-to-protein interaction, complexes from the GST pull-down in Fig. 5 were analyzed by western blot using an antibody against ARTD1. Since the loss-of-binding mutants and GST do not interact with ARTD1 they were used as negative controls for the following experiments.

4.1.6 Comparison to a mass spectrometry compatible stain

A mass spectrometry compatible staining solution with a high sensitivity, as recommended by the Functional Genomics Center, was used to stain the samples of the GST pull-down described above in section 4.1.4 (Fig. 7).

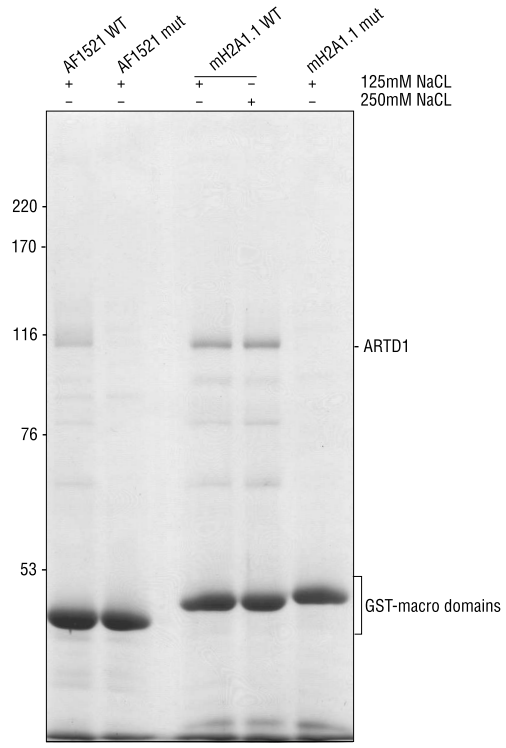

Figure 7. 7.5% SDS-PAGE, Roti blue (Roth) colloidal G-250 Coomassie blue stain.

Although the sensitivity is high, interaction partners are less easy to identify than on a silver stain. Therefore further GST pull-downs were still first analyzed by silver stain, but an aliquot was stored for mass spectrometry.

4.1.7 ARTD1 from untreated RAW-264.7 extracts binds to mH2A1.1 and mD2, but not to the expressed BAL *macro* domains

Since ARTD1 was previously described as interaction partner of the proteins AF1521 and mH2A1.1, we wanted to investigate its co-precipitation properties with the ARTD7–9 *macro* domains and mD2.

To investigate the binding partners of BAL *macro* domains, GST pull-downs were performed with untreated RAW264.7 extracts. Afterwards co-purified proteins were separated by SDS-PAGE and analyzed by silver staining. To assess, whether the expressed BAL *macro* domains bind mono- or poly-ADP-ribosylated endogenous ARTD1, the *macro* domain mD2 was included as a mono-ADP-ribose binding positive control, and the co-purified proteins were analyzed by ARTD1 western blot (Fig. 8).

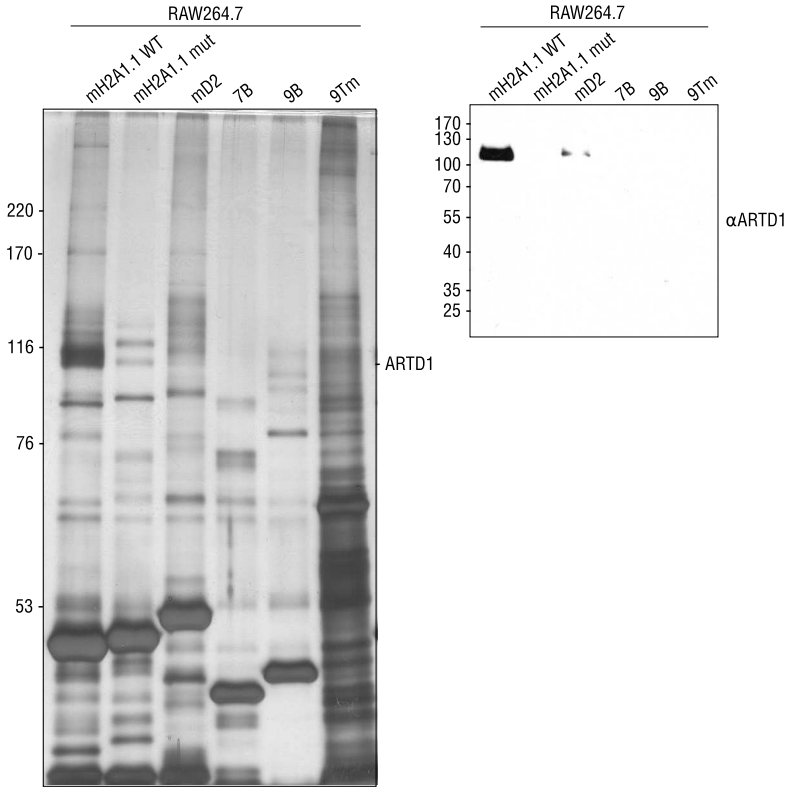

Figure 8. Untreated RAW-264.7 extracts were used for GST *macro* domain pull-downs. Left panel: Co-purified proteins were separated by 7.5% SDS-PAGE and silver stained. Right panel: The same samples were analyzed by western blot against ARTD1.

This revealed that mD2 binds endogenous ARTD1, although to a lesser extent than mH2A1.1. Conversely, endogenous ARTD1 was not detected in the complexes formed by the analyzed BAL *macro* domains. Further GST pull-downs were performed with stimulated extracts to analyze, if this is a detection-, treatment- or cell line-specific characteristic of BAL *macro* domains.

4.1.8 ARTD1 from LPS treated RAW-264.7 extracts binds to mH2A1.1 and mD2, but not to the expressed BAL *macro* domains

GST pull-downs were performed with LPS-treated RAW264.7 extracts, to further investigate the binding partners of the expressed BAL *macro* domains. Cells were treated for 4 h with 100 ng/mL *E. coli* lipopolysaccharides (LPS) to induce mono- and poly-ADP-ribosylation (cf. the ARTD1-smear in Fig. 10, which indicates PAR formation, to the ARTD1 band in Fig. 8), thereafter extracts were prepared. Then the GST pull-down was performed. Co-purified proteins were separated by SDS-PAGE and analyzed by silver staining and the indicated bands were selected for identification by mass spectrometry (Fig. 9).

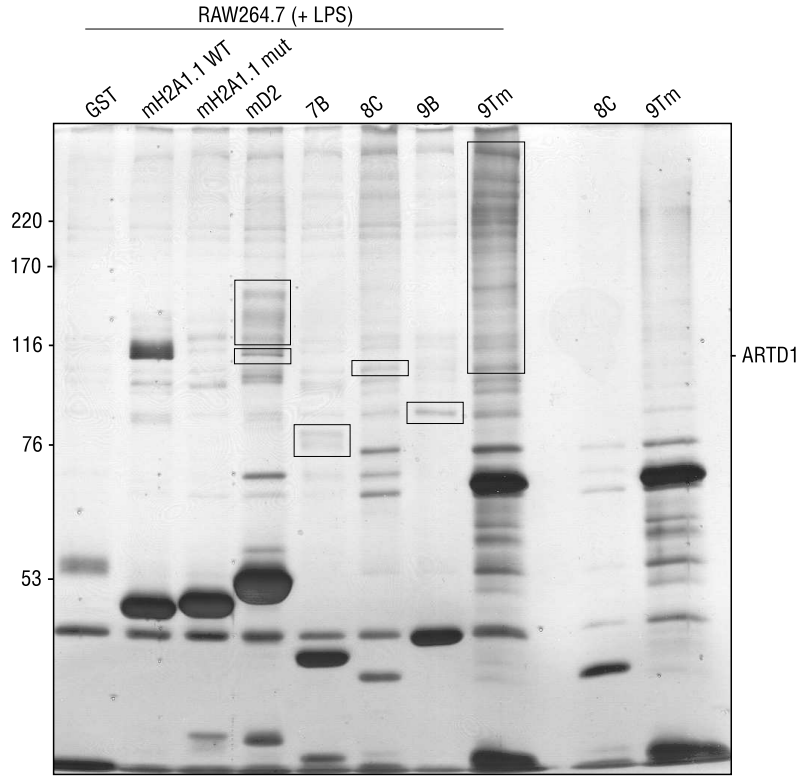

Figure 9. LPS treated RAW-264.7 extracts were pulled down with resin-bound GST *macro* domains. Co-purified proteins were separated by 7.5% SDS-PAGE and silver stained. On the two lanes to the right rebound GST *macro* domains without addition of RAW-264.7 extracts are loaded as additional negative controls. The indicated bands were selected for identification by mass spectrometry.

To assess, whether BAL *macro* domains bind mono- or poly-ADP-ribosylated endogenous ARTD1, the co-purified proteins were analyzed by ARTD1 western blot (Fig. 10).

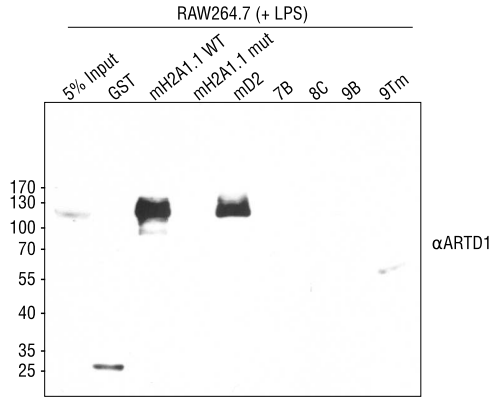

Figure 10. Western blot analysis with an anti-ARTD1 antibody. The same samples as analyzed by silver stain and shown in Fig. 9 were used.

Again, western blot anti-ARTD1 revealed that mD2 binds endogenous ARTD1, although to a lesser extent than mH2A1.1. Reproducibly, endogenous ARTD1 could not be detected in the complexes co-purified with the analyzed BAL *macro* domains.

4.1.9 ARTD1 from H_2O_2 treated U-2932 extracts binds to mH2A1.1 and mD2, but not to the expressed BAL *macro* domains

BAL proteins were originally identified in DLBCL. We therefore assessed the interaction of the expressed *macro* domains with extracts from the U-2932 cell line. GST pull-downs were repeated with H_2O_2 treated U-2932 DLBCL cell extracts. H_2O_2-treatment was used to enhance mono- and poly-ADP-ribosylation of possible binding partners (11).

In a preliminary experiment, PAR formation after H_2O_2-treatment was analyzed by western blotting (Fig. 11).

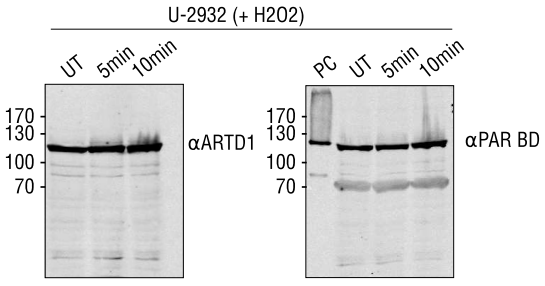

Figure 11. Western blot analysis anti-ARTD1 and anti-PAR. U-2932 cells were incubated with medium containing 1mM H_2O_2 for the indicated period. WCE were prepared, separated by 7.5% SDS-PAGE and analyzed by western blot. PC indicates a PAR positive control.

PAR formation was treatment and time dependent with a maximum at time point 10 min. Interestingly, also in untreated cells PAR formation was visible, although to a minor extent. For the

following GST pull-down experiment, U-2932 cells were therefore treated for 10 min with 1mM H_2O_2. Co-purified proteins were separated by SDS-PAGE and analyzed by silver staining (Fig. 12).

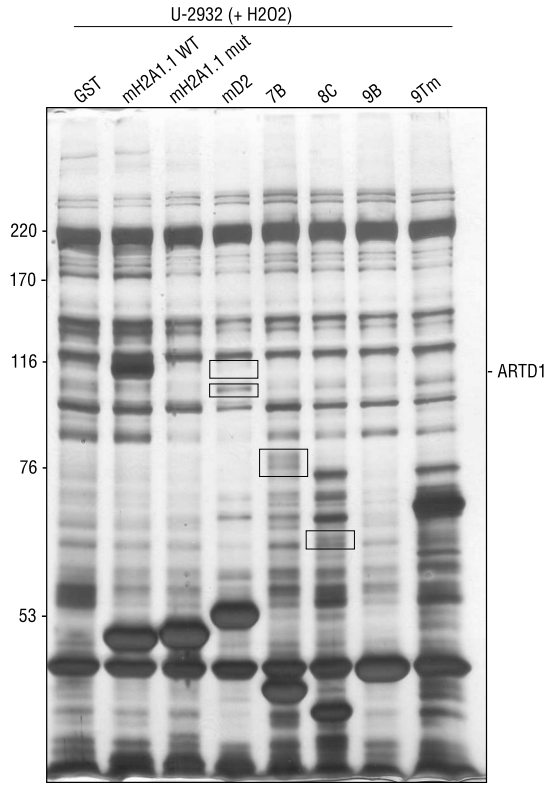

Figure 12. H_2O_2 treated U-2932 extracts were pulled down with resin-bound GST *macro* domains. Co-purified proteins were separated by 7.5% SDS-PAGE and silver stained. The indicated bands were selected for identification by mass spectrometry.

To assess, whether BAL *macro* domains bind mono- or poly-ADP-ribosylated endogenous ARTD1, the co-purified proteins were again analyzed by ARTD1 western blot (Fig. 13).

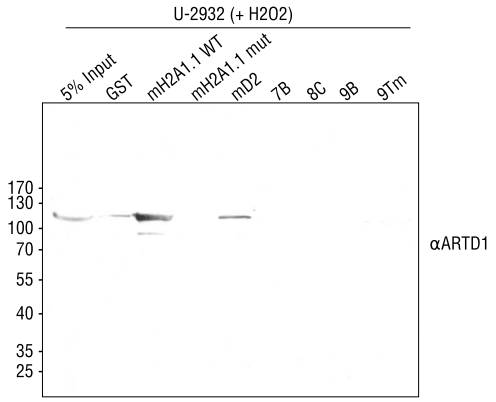

Figure 13. Western blot analysis with an anti-ARTD1 antibody. The same samples as analyzed by silver stain and shown in Fig. 12 were used.

Western blot anti-ARTD1 revealed that mD2 binds endogenous ARTD1, although to a lesser extent than mH2A1.1. Reproducibly, the analyzed BAL *macro* domains didn't bind endogenous ARTD1 at all.

4.1.10 Identification of *macro* domain specific interaction partners by tandem mass spectrometry

The gel bands indicated in Fig. 9 were cut and sent to the Functional Genomics Centre Zurich (FGCZ). The interaction partners identified by LC/ESI/MS/MS at the FGCZ are listed in Table 4.1. Significant hits (Protein probability > 95% as analyzed by Scaffold) for each *macro* domain are listed above the black line. Proteins validated as interaction partners by western blot are indicated by a plus (+) sign. Proteins with no entry in the validation column were not verified by western blot.

A first overview revealed that the proteins tubulin, vimentin, nucleolin and heat shock cognate 71 protein were found to be interacting with ARTD9/BAL1 tandem (9Tm), ARTD7 and ARTD8 *macro* domains. These proteins were previously described to be ADP-ribosylated and to be interaction partners of ARTD1 (11, 37, 127, 128). This provided the first evidence that the established experimental setup was working in the anticipated way. The method was therefore used for further experiments.

As deduced from the multiple sequence alignment (cf. paragraph 4.1.1), distinct binding properties were expected for the different *macro* domains. ARTD1 was only detected as interaction partner of mD2, but not of the other analyzed *macro* domains, underlining the previously conducted analysis by western blot (cf. paragraph 4.1.8). p62/sequestosome-1, a protein involved in selective autophagy and mutated in Paget's disease of the bone, was specifically detected as interaction partner of 9Tm.

Another group of proteins detected comprises RNA associated helicases and heterogenous nuclear ribonucleoproteins (HNRPs) A/B, F, U and M. These proteins were previously found to be associated with ARTD1 and are thought to interact unspecifically by binding to nucleic acids. To test this hypothesis, the interaction between p68/RNA helicase DDX5 and the ARTD9/BAL1 was reanalyzed by co-immunoprecipitation with addition of ethidium bromide (EtBr). EtBr abrogates the nucleic acid-mediated interaction between proteins through intercalation and can therefore remove false positive interaction partners in a pull-down assay (129).

Plasminogen Activator Inhibitor 1 RNA binding protein, Immune responsive gene 1, RuvB-like 1, Zinc finger CCCH-type antiviral protein 1 (ZAP/ARTD13) and 54 kDa 2'-5'-oligoadenylate synthase-like protein 2 form an antiviral cluster (130, 131). The gene of 2'-5'-oligoadenylate synthase-like protein 2 was previously found to be upregulated upon ARTD9 overexpression (43). The detection of the mentioned proteins as interaction partners underlines the antiviral properties of *macro* ARTD 9 and 8.

Table 4.1. Protein identification by LC/ESI/MS/MS, Functional Genomics Centre Zurich (FGCZ). Identification of BAL *macro* domain interaction partners by tandem mass spectrometry. Significant hits (Scaffold probability > 95%) for each *macro* domain are listed above the black lines.

Protein	Accession	Peptides	Mass in kDa	Validation
ARTD9/BAL1 tandem macro				
β-Tubulin	P07437	13	50	
Nucleolin	P09405	11	77	+
Plasminogen Activator Inhibitor 1 RNA binding protein	Q6AXS5	3	45	
Heterogenous nuclear ribonucleoprotein U	Q00839	2	91	
Tubulin α-1B chain	P05213	2	50	
Heterogenous nuclear ribonucleoprotein F	P52597	1	46	
Sequestosome-1	Q64337	1	48	+
ATP dependent RNA helicase DDX3X	O00571	1	73	
Nucleolar RNA helicase 2	Q3B8Q1	1	86	
Immune responsive gene 1	P54987	1	54	
RuvB-like 1	P60122	1	50	
Heterogenous nuclear ribonucleoprotein M	Q9D0E1	1	78	
ARTD13/Zinc finger CCCH-type antiviral protein 1	Q3UPF5	1	107	+
ARTD8/BAL2 macro C				
Nucleolin	P09405	14	77	+
Vimentin	P20152	6	59	
β-Tubulin	P07437	3	50	
Heterogenous nuclear ribonucleoprotein U	Q00839	3	91	
Nucleolar RNA Helicase 2	Q9JIK5	3	94	
60S acidic ribosomal protein P0	P14869	2	34	
p68/Probable ATP-dependent RNA helicase DDX5	A5A6J2	2	69	+
Heterogenous nuclear ribonucleoprotein A/B	Q99020	1	31	
RuvB-like 1	P60122	1	50	
Immune responsive gene 1	P54987	1	54	
Heterogenous nuclear ribonucleoprotein M	Q9D0E1	1	78	
ATP-dependent RNA Helicase DDX24	Q9ESV0	1	94	
ARTD9/PARP9/BAL1	Q8IXQ6	1	96	
ARTD13/Zinc finger CCCH-type antiviral protein 1	Q3UPF5	1	107	
Plasminogen Activator Inhibitor 1 RNA binding protein	Q6AXS5	1	45	
54 kDa 2'-5'-oligoadenylate synthase-like protein 2	Q9Z2F2	1	55	
Sphingosine-1-phosphate lyase 1	A8R0X7	1	64	
ARTD7/BAL3 macro B				
Heat shock cognate 71	A2Q0Z1	1	71	
Macro D2				
ARTD1/PARP1	P11103	1	113	+

Interestingly, ARTD9 could be detected as interaction partner of the ARTD8 *macro* domain. This signifies that the *macro* domain containing ARTDs do not necessarily act alone, but can also form dimers. This observation is in line with previously published data indicating that ARTD proteins

can trans-modify each other (132, 133).

Validation of mass spectrometry results by western blot

Protein complexes from GST *macro* domain 9Tm and mD2 pull-downs with LPS treated RAW-264.7 extracts were analyzed by western blot in order to validate the interaction partners identified by mass spectrometry. In Fig. 14 western blots with antibodies against nucleolin, ARTD10 and ARTD13 are shown.

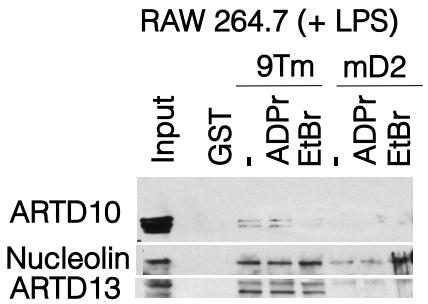

Figure 14. LPS treated RAW-264.7 extracts were pulled down with the indicated resin-bound GST *macro* domains. Washed complexes were separated according to molecular weight on a 10% SDS-PAGE and analyzed by western blotting with antibodies against ARTD10, ARTD13 and nucleolin. EtBr and ADPr indicate the addition of ethidium bromide (EtBr) or ADP-ribose (ADPr) to the pull-downs.

Ethidium bromide (EtBr) added to pull-down reactions was previously described to abrogate interactions mediated by nucleic acids. The interaction between 9Tm and ARTD10 was interrupted by EtBr and was therefore considered to be mediated by nucleic acids. In contrast, the interactions with nucleolin and ARTD13 were specific. In both cases, ADP-ribose (ADPr) addition could not interrupt the interaction. This could identicate that the interaction is either not mediated by ADPr or that free ADPr binds with lower affinity to the *macro* domain 9Tm.

In order to exclude that the observed interactions are mediated by bacterial bridging factors, HA-co-immunoprecipitations were done with extracts from human A549 cells expressing empty vector or HA-ARTD9. This approach verified at the same time that the bacterially expressed fusion proteins are folded correctly. To investigate, if ADP-ribosylation has an effect on the interaction, one half of the cells was treated with LPS before preparing whole cell extracts. Using this assay, ARTD1, nucleolin and the RNA helicase DDX5/p68 were verified as interaction partners of full length ARTD9 (Fig. 15), as well as ARTD13 and p62 (Fig. 16).

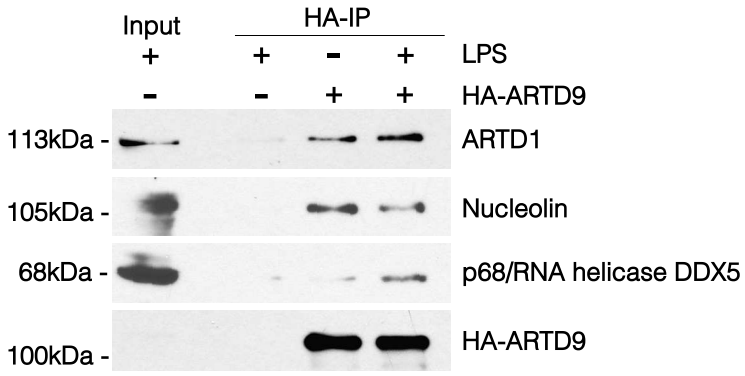

Figure 15. Extracts from A549 cells stably expressing HA-ARTD9 or an empty vector were co-immunoprecipitated with HA-agarose. A549 cells were previously treated with LPS to stimulate ADP-ribosylation. Washed complexes were separated according to molecular weight on a 10% SDS-PAGE and analyzed by western blotting with antibodies against ARTD1, nucleolin and p68.

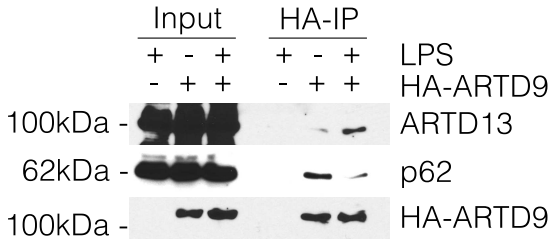

Figure 16. Extracts from A549 cells stably expressing HA-ARTD9 or an empty vector were co-immunoprecipitated with HA-agarose. A549 cells were previously treated with LPS to stimulate ADP-ribosylation. Washed complexes were separated according to molecular weight on a 10% SDS-PAGE and analyzed by western blotting with antibodies against ARTD13 and p62.

p62 was the strongest interaction partner of ARTD9 as assessed by western blot. LPS-stimulation increased the amount of ARTD1, ARTD13 and p68 bound to ARTD9. In contrast, p62 and nucleolin co-immunoprecipitated at lower levels, when cells were treated with LPS, then observed under untreated conditions.

Ethidium bromide (EtBr) was added to the HA-immunoprecipitation reactions to further characterize the nature of the interaction between ARTD9 and p62. As described above, ethidium bromide abrogates interactions mediated by nucleic acids in pull-down assays. The interaction between ARTD9 and p62 could not be interrupted by addditon of EtBr (Fig. 17).

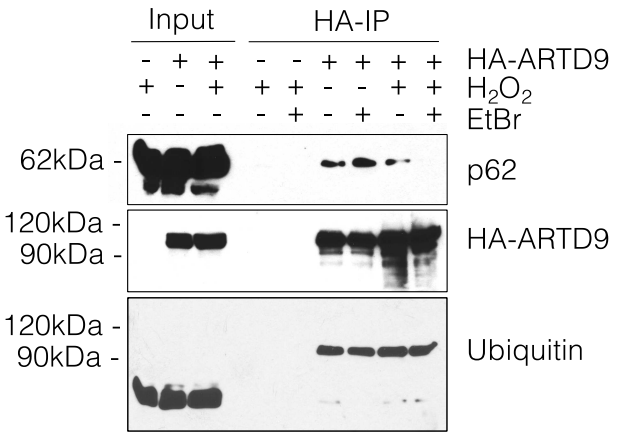

Figure 17. Extracts from A549 cells stably expressing HA-ARTD9 or an empty vector were co-immunoprecipitated with HA-agarose. A549 cells were previously treated with H_2O_2 to stimulate ADP-ribosylation where indicated. Complexes were washed, separated according to molecular weight on a 10% SDS-PAGE, and analyzed by western blotting with antibodies against HA and p62 and ubiquitin. EtBr indicates the addition of ethidium bromide to the pull-downs.

This provides evidence that the interaction between ARTD9 and p62 is not mediated by nucleic acids and therefore can be considered specific.

To investigate and reproduce the observed effect of ADP-ribosylation induced by LPS (cf. Fig. 16), the cells were additionally treated with H_2O_2, a strong ADP-ribosylation inducer, before preparation of extracts. H_2O_2 likewise reduced the interaction between ARTD9 and p62.

The complexes were also analyzed with an ubiquitin antibody, since mono-ubiquitinylation is a prerequisite for proteins to bind p62 and further degradation by selective autophagy. This western blot reveals that at least a subfraction of ARTD9 is mono-ubiquitinylated.

In summary, the above data indicate that p62 interacts ARTD9 over its *macro* domains. The interaction could not be interrupted by EtBr. Additionally, a subfraction of ARTD9 was shown to be mono-ubiquitinylated.

4.2 ARTD9 and autophagy

Since p62 is involved in several cellular processes including autophagy (see introduction), we were curious if the interaction between ARTD9 and p62 has functional consequences. Thus, an experimental setup to induce and monitor autophagy A549 cells was established.

4.2.1 Starvation induces autophagy in A549 cells

To induce autophagy in A549 cells, serum starvation was chosen, a well known autophagy inducer. Starved A549 cells were harvested after the indicated time and whole cell extracts were analyzed by western blot with antibodies against phospho-p70S6 kinase (p-p70S6K), phospho-AMP kinase (p-AMPK) and LC3B (Fig. 18).

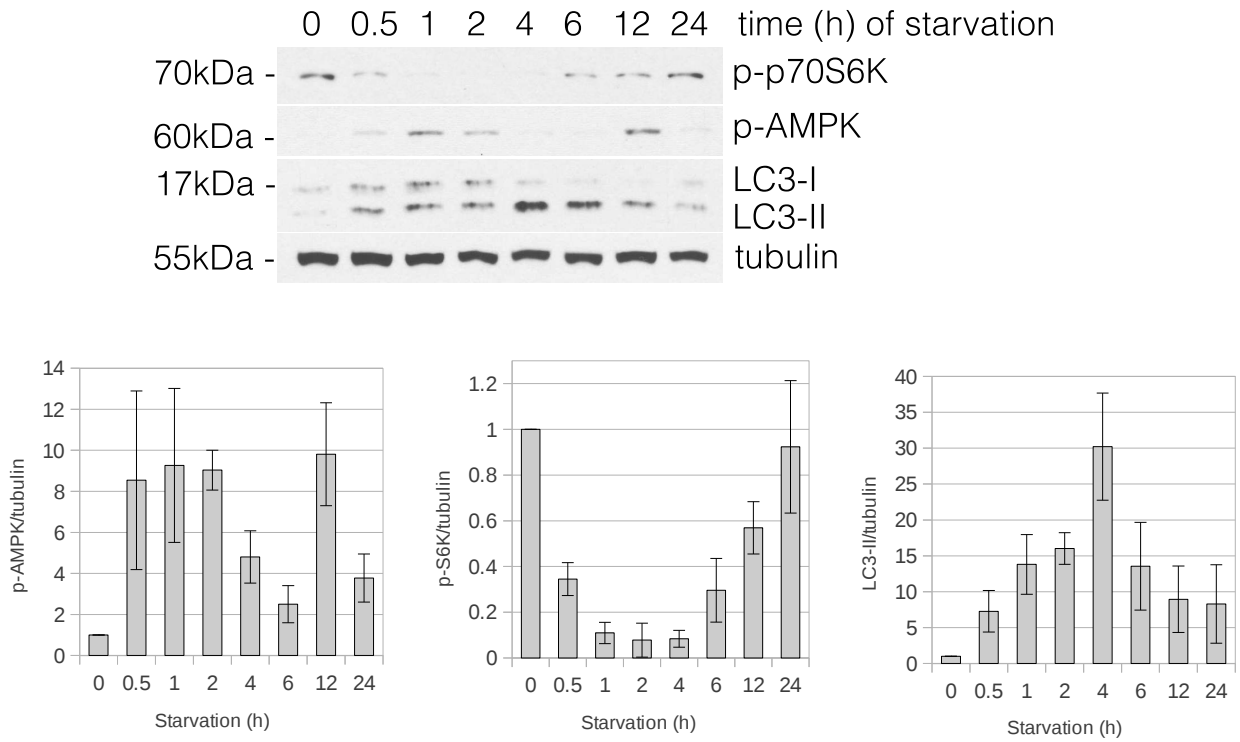

Figure 18. Time-course of starvation induced autophagy in A549 cells. Upper part: A549 cells were washed twice to remove remaining fetal calf serum (FCS) and thereafter incubated for the indicated time in starvation medium (serum-free DMEM). WCE were prepared and analyzed by western blotting with antibodies against phospho-p70S6 kinase (p-p70S6K), phospho-AMP kinase (p-AMPK) and LC3B. Tubulin served as loading control. Lower part: the corresponding quantification is depicted. Values are expressed relative to 0h (control). Error bars represent standard deviation (SD), $n = 3$.

Already after 0.5–1 h of starvation AMP kinase (AMPK) is phosphorylated, followed by the inactivation of mTOR, which in turn de-phosphorylates p70S6 kinase (p70S6K). LC3B-II, a marker of autophagic membrane, is detected in increased levels already after 0.5–1 h and shows a peak after 4–6 h of starvation in A549 cells. After 4 h starvation AMPK phosphorylation is decreased again, most probably due to ATP accumulation as result of induced autophagy. A second wave of phosphorylation is initiated with the phosphorylation of AMPK at time point 12 h.

In summary, starvation induces autophagy in A549 cells in a time dependent manner. The established experimental approach worked in the anticipated way. It allows to monitor autophagy, by observation of autophagic signaling markers. The method was therefore used for further experiments.

4.2.2 Autophagy decreases ARTD9 levels in A549 cells

The next step was to explore, if induction of autophagy influences ARTD9 levels or if ARTD9 has an effect on autophagy. This was carried out by using A549 cells stably expressing an empty vector or full length human ARTD9 tagged with the hemagglutinin (HA) epitope tag. The cells were incubated for the indicated duration in starvation medium, and extracts were analyzed by western blot. A first overview reveals that basal autophagy is not significantly altered by ARTD9. No difference could be detected between LC3B-II levels of untreated A549 empty and A549 HA-ARTD9 cells (Fig. 19, 0 h lanes).

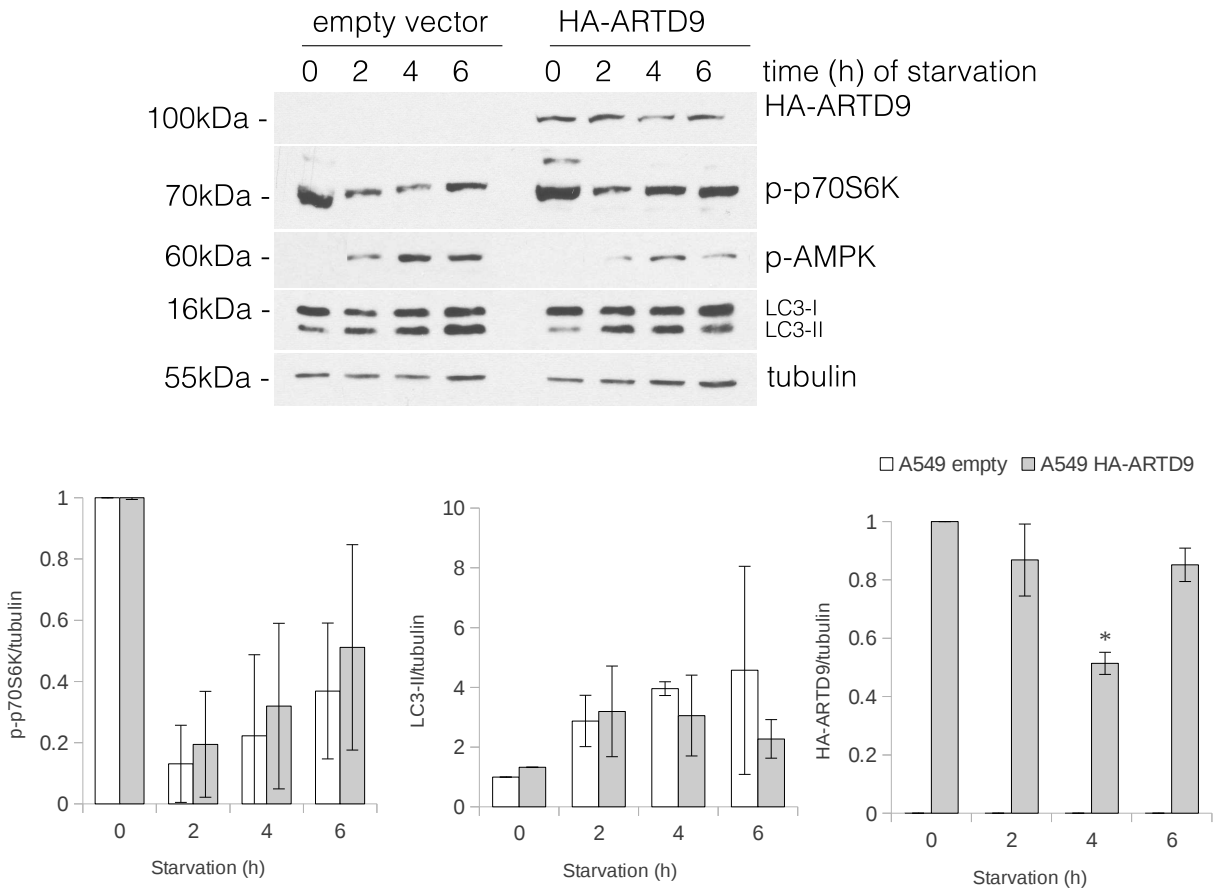

Figure 19. Time-course of autophagy induction in serum starved A549 empty and A549 HA-ARTD9 cells. Upper part: cells were washed twice to remove remaining FCS and thereafter incubated for the indicated time in starvation medium. WCE were prepared and analyzed by western blotting with antibodies against hemagglutinin (HA), phospho-p70S6 kinase (p-p70S6K), phospho-AMP kinase (p-AMPK) and LC3B. Tubulin was used as loading control. Lower part: the corresponding quantification is shown. Values are expressed relative to 0h (control). $n = 3$, error bars represent SD, * indicates $p < 0.05$, Student's t-test.

The same holds true for induction of autophagy, as assessed by LC3B-II levels and AMPK and p70S6K phosphorylation as well. In contrast, ARTD9 protein levels are significantly decreased ($p < 0.05$) by 40% after 4 h starvation.

To further investigate and reproduce the observed effect of starvation induced autophagy on ARTD9, A549 empty and A549 HA-ARTD9 cells were starved for prolonged durations (Fig. 20).

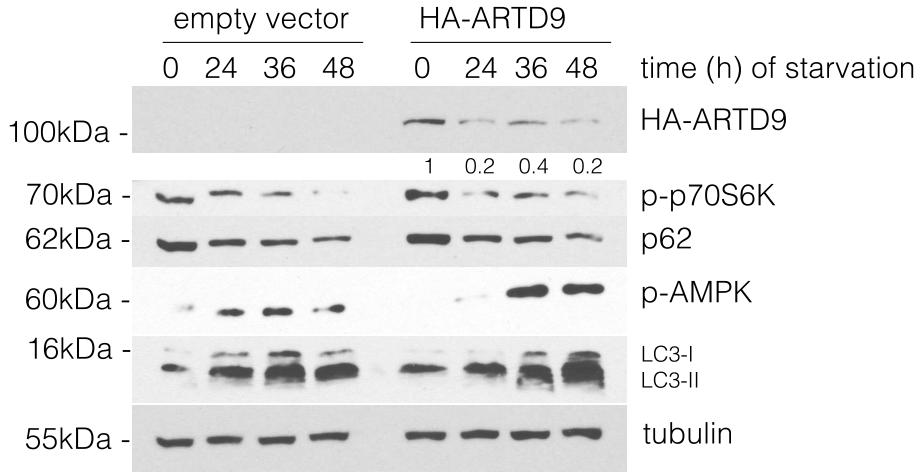

Figure 20. Time-course of autophagy induction in serum starved A549 empty and A549 HA-ARTD9 cells. Cells were washed twice to remove remaining FCS and thereafter incubated for the indicated time in starvation medium. WCE were prepared and analyzed by western blotting with antibodies against hemagglutinin (HA), p62, phospho-p70S6 kinase (p-p70S6K), phospho-AMP kinase (p-AMPK) and LC3B. Tubulin served as loading control. The values below the HA immunoblot indicate the level of HA-ARTD9 (normalized to tubulin) relative to 0h (control).

p62 functions as adaptor protein and substrate for selective autophagy and is therefore constantly degraded. As described, its levels negatively correlated with LC3B-II levels.

In summary, markers for starvation induced autophagy in A549 were not significantly influenced by HA-ARTD9, but prolonged starvation decreased HA-ARTD9 protein levels by 80%.

4.2.3 ARTD9 messenger RNA levels in A549 cells after starvation

To ascertain that this starvation induced decrease of HA-ARTD9 protein levels was not due to decreased transcript levels of HA-ARTD9, ARTD9 messenger RNA was measured by reverse transcription real time polymerase chain reaction (RT real time PCR). After the indicated duration of starvation, ARTD9 mRNA levels were equal or higher than in the control samples (Fig. 21, 0 h).

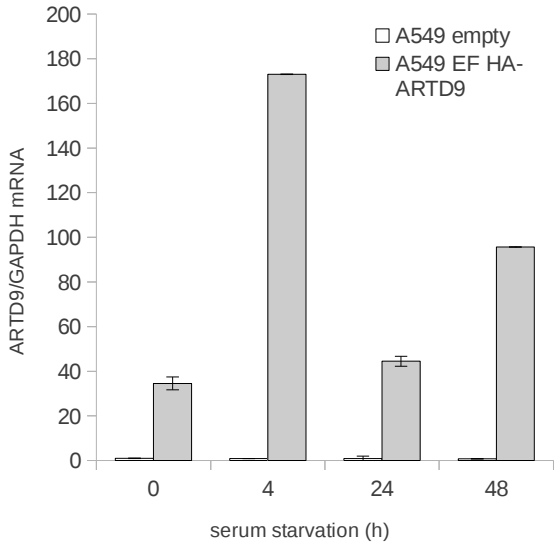

Figure 21. ARTD9 messenger RNA levels are equal or upregulated after serum starvation. Cells were washed twice to remove remaining FCS and thereafter incubated for the indicated time in starvation medium. Total RNA was prepared and reverse transcribed. ARTD9 mRNA levels were analyzed by real time PCR according to the $2^{-\Delta Ct}$ method and normalized to GAPDH mRNA. Values express the level of HA-ARTD9 relative to 0 h (control). Error bars represent standard deviation (SD), $n = 2$.

This is consistent with a previous study, where the EF-1α promoter was described to be upregulated by serum starvation in *A. albopictus* mosquito cells (134).

Altogether, this indicates that the observed decrease of ARTD9 protein after starvation can not be explained by reduced transcript levels and is most likely caused by induced autophagy.

4.2.4 siRNA mediated knockdown of p62 in A549 cells

After having established that (a) ARTD9 and p62 interact and (b) induction of autophagy decreases ARTD9 protein levels, we examined if it would be possible to abrogate this effect by siRNA mediated gene silencing of p62. For this reason, A549 cells stably expressing HA-ARTD9 were treated with control and p62 siRNA and analyzed by western blot for p62 and HA-ARTD9 (Fig. 22).

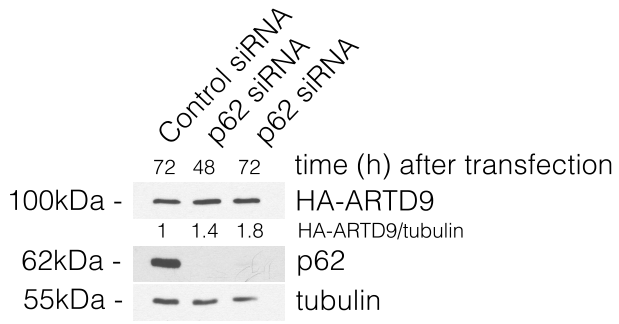

Figure 22. 48h after silencing p62 is not detectable by western blot anymore while HA-ARTD9 levels appear increased under basal conditions. WCE were prepared and analyzed by western blotting with antibodies against hemagglutinin (HA) and p62. The values below the HA immunoblot indicate the level of HA-ARTD9 (normalized to tubulin) relative to control. Tubulin served as loading control. The experiment was performed once.

Tubulin was used as loading control. 48h after silencing p62 was not anymore detectable by western blot while HA-ARTD9 levels appeared increased under basal conditions.

Next, the cells silenced for p62 were starved for the indicated durations, to verify, if the p62 knockdown also abrogates the observed decrease of ARTD9 protein after starvation. Again, WCE were prepared and analyzed by western blot (Fig. 23).

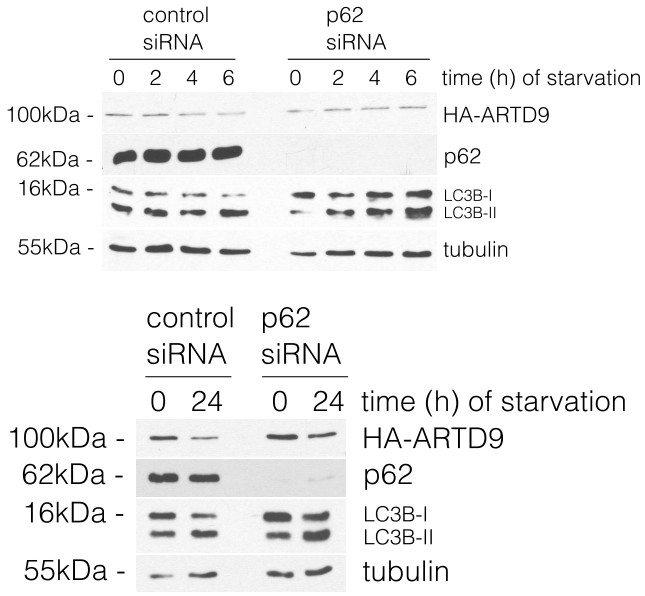

Figure 23. HA-ARTD9 levels in p62-silenced cells appear not to decrease after starvation. Cells were washed twice to remove remaining FCS and thereafter incubated for the indicated time in starvation medium. WCE were prepared and analyzed by western blotting with antibodies against hemagglutinin (HA), p62, beclin-1, phospho-p70S6 kinase (p-p70S6K), and LC3B. Tubulin served as loading control. The experiment was performed twice.

Silencing of p62 did not abrogate the induction of autophagy by serum starvation as analyzed by the marker LC3B-II. The HA-ARTD9 levels in cells treated with the control siRNA were decreased

after starvation as observed in previous experiments. In contrast, in cells silenced for p62 the starvation induced decrease of HA-ARTD9 could not be observed (2–6 h starvation) or was reduced (24 h starvation).

In summary, the experimental data give a hint that ARTD9 interacts with p62 and is degraded by selective autophagy.

4.2.5 siRNA mediated knockdown of beclin-1 in A549 cells

Beclin-1 was silenced by siRNA mediated gene silencing, to further characterize the subpathway involved in the degradation of ARTD9 by autophagy. For this reason, A549 cells stably expressing HA-ARTD9 were treated with control and beclin-1 siRNA and analyzed by western blot for beclin-1, p62 and HA-ARTD9 (Fig. 24).

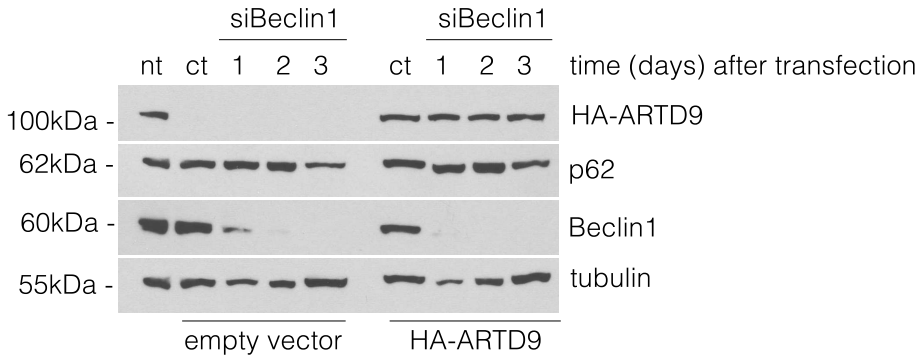

Figure 24. Beclin-1 silencing. 72h after silencing beclin-1 is not detectable by western blot anymore. WCE were prepared and analyzed by western blotting with antibodies against hemagglutinin (HA), beclin-1 and p62. Tubulin served as loading control. The experiment was performed once.

Tubulin was used as loading control. 72h after silencing, beclin-1 was not anymore detectable by western blot, but HA-ARTD9 levels appeared not influenced under basal conditions.

To investigate, if the beclin-1 knockdown might influence the observed decrease of ARTD9 protein after starvation, the cells silenced for beclin-1 were starved for the indicated time. WCE were prepared and analyzed by western blot (Fig. 25).

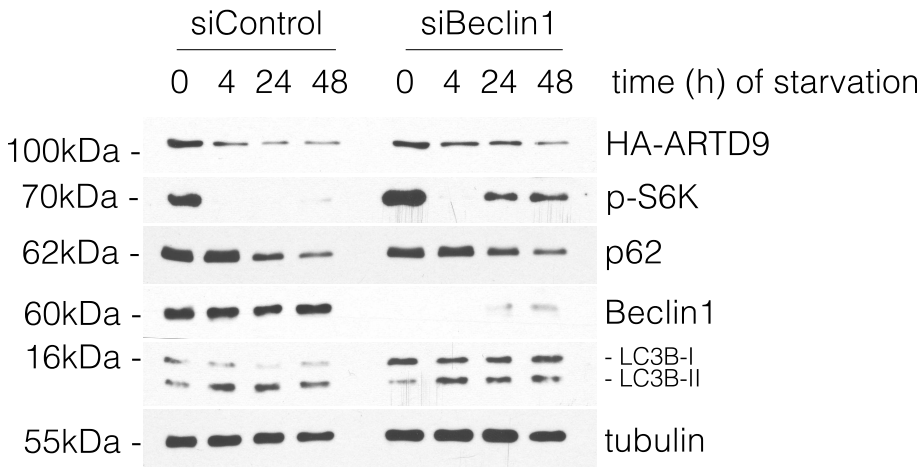

Figure 25. Beclin-1 silencing does not alter the observed autophagy induction, nor the degradation of HA-ARTD9 or p62. Cells were washed twice to remove remaining FCS and thereafter incubated for the indicated time in starvation medium. WCE were prepared and analyzed by western blotting with antibodies against hemagglutinin (HA), p62, beclin-1, phospho-p70S6 kinase (p-p70S6K), and LC3B. Tubulin served as loading control. The experiment was performed once.

Silencing of beclin-1 did not abrogate the induction of autophagy by serum starvation in A549 cells as analyzed by the marker LC3B-II and the observed decrease of p62. The HA-ARTD9 levels in cells treated with the control siRNA and siRNA against beclin-1 were decreased after starvation as observed in previous experiments.

In summary, the experimental data suggest that starvation induced autophagy in A549 cells is beclin-1 independent.

5 Discussion

The aim of this project was to establish an unbiased approach to identify and functionally characterize binding partners of both the full length *macro*ARTD proteins as well as their respective single and tandem *macro* domains. Therefore, single and tandem *macro* domains cloned into the pETM33 vector were expressed as His-GST fusion proteins in *E. coli*. Subsequently, GST pull-downs were performed and the co-purified proteins were separated by SDS-PAGE and analyzed by silver staining. The bands representing probable interaction partners were selected for identification by mass spectrometry. The identified proteins where then validated by further GST pull-downs and HA-immunoprecipitations analyzed by western blot.

Previously, ARTD1 was shown as interaction partner of several *macro* domain containing proteins, namely AF1521, mH2A1.1 and ALC1 (33, 35, 36, 38). Since macroD2 bound mono-ADP-ribose with high affinity, but did not bind PAR efficiently (29), we included it in the set of parallel pull-downs as a mono-ADP-ribose binding control. To investigate, if BAL *macro* domains have different binding properties as single or in tandem, we also expressed 9Tm, the tandem *macro* domains of ARTD9.

Thereafter, we performed GST *macro* domain pull-downs with unstimulated and LPS stimulated RAW-264.7 extracts. The analysis of the silver stained gels shows differing band patterns between the different *macro* domains. Differences exist also between single and tandem *macro* domains. Additionally, we discovered that mD2 interacts with ARTD1, using western blots to identify ARTD1, but no interaction of the expressed BAL *macro* domains with ARTD1 could be detected under the observed conditions. In addition, these results are consistent with the ones inferred from the multiple sequence alignment. To rule out a cell line specific effect, the GST pull-downs were repeated with extract of the U-2932 cell line. This time we used H_2O_2 treatment to induce mono- and poly-ADP-ribosylation. But again, western blotting against ARTD1 revealed no interaction of the expressed BAL *macro* domains with ARTD1 under the observed conditions. Also by mass spectrometry, ARTD1 could only be detected as interaction partner of mD2, but not as interaction partner of the expressed BAL *macro* domains. If the expressed BAL *macro* domains might be incorrectly folded, in contrary to the *macro* domains mH2A1.1 and mD2 expressed under the same conditions, is described in the paragraphs below.

EtBr was added to the pull-downs and HA-immunopreciptiations to abrogate interactions mediated by nucleic acids, in an attempt to eliminate false positive interaction partners. Using this method, nucleolin and ARTD13 could be detected as specific interaction partners of 9Tm.

Hemagglutinin (HA)-tagged full length ARTD9 protein was stably expressed in (human) A549 cells for three reasons. First, to exclude that the identified interactions with the *macro* domains are mediated by bacterial contamination functioning as bridging factor. Second, to rule out that the interaction partners identified are unspecific due to incorrect folding of the recombinantly expressed *macro* domain proteins. Third, it also served to additionally reproduce and investigate the observed interaction partners of the GST *macro* domains with the full length ARTD9/BAL1 protein by HA-immunoprecipitation.

Using this approach, p62, ARTD13, nucleolin and p68/DDX5 were validated as interaction partners of ARTD9. Unexpectedly, ARTD1 could be detected as interaction partner of ARTD9 by western blot, as well. This data could be explained by the difficulty to ionize peptides of ARTD1 during mass spectrometry (personal communication P. O. Hassa). Another explanation would be that the western blot against ARTD1 was developed using Pierce SuperSignal West Pico, an enhanced chemiluminescence substrate with higher sensitivity than the previously used Pierce ECL. Another explanation could be that the interaction of ARTD9 with ARTD1 is not mediated by the tandem *macro* domains of ARTD9. Since the interactions between recombinantly expressed 9Tm and ARTD13, p68/DDX5, nucleolin and p62 could be reproduced with full length ARTD9, the possibility that the BAL *macro* domains are incorrectly folded appears unlikely.

The interaction between p62 and ARTD9 was the strongest, as observed by western blot. Since p62 is an adapter protein targeting ubiquitinylated proteins for degradation by selective autophagy, we analyzed, if ARTD9 is ubiquitinylated,. Indeed, a subfraction of ARTD9 was proven to be mono-ubiquitinylated, as analyzed by an anti-ubiquitin western blot.

We then asked, if the interaction of ARTD9 with p62 has functional implications. The effect of induced autophagy on ARTD9 was investigated, since a subfraction of ARTD9 is mono-ubiquitinylated and p62 targets ubiquitinylated proteins to the lysosome. Serum starvation as a well known inducer of autophagy was used to treat A549 cells expressing HA-ARTD9. Induction of autophagy was verified by the analysis of several markers including LC3 turnover. Using this assay, HA-ARTD9 protein levels were reduced significantly by 40% after 4 h starvation. The degradation rate found for ARTD9 in this study is comparable to the one found recently for the connexins CX43 and CX50 (135).

To investigate if this decrease is p62 dependent, p62 was silenced by siRNA mediated gene silencing. Using siRNA against p62, the observed reduction of ARTD9 could be abolished and basal ARTD9 levels were increased although autophagy could still be induced in A549 cells. This provides evidence that the observed decrease of ARTD9 after starvation-induced autophagy is indeed p62 dependent.

To characterize the autophagy pathway responsible for degradation of ARTD9, Beclin-1 was then silenced by siRNA mediated gene silencing. Basal ARTD9 levels as well as the starvation induced autophagy were not affected by the Beclin-1 knockdown in A549 cells. This suggests that ARTD9 is degraded by p62 dependent but beclin-1 independent selective autophagy, since siRNA-mediated

silencing of beclin-1 could not inhibit autophagy in A549 cells as well as the observed decrease of ARTD9 and p62.

As mentioned above (see Introduction, section 1.1.3), ARTD9/BAL1 was reported as co-activator of STAT1 and repressor for IRF1, an important IFNγ induced target gene of STAT1 (50). At the same time, IFNγ induces autophagy and the expression of ARTD9/BAL1 as well (see Introduction, section 1.4 and 1.1.2 for details). p62 is a signaling adaptor and interacts with atypical protein kinase C (PKC), thereby positively regulating NF-κB mediated cytokine signaling downstream of various receptors (136). Recently, the degradation of BCL10 by p62-dependent selective autophagy was reported to protect T cells from aberrant NF-κB signaling in an analogous manner (137). This prompts speculation that p62 could also be required for activation of IFNγ/STAT1 signaling cascades in a similar way.

On the other hand, ARTD9/BAL1 degradation by selective autophagy could also be a negative feedback loop to modulate IFNγ/STAT1 signaling. ARTD9 is detected 6-12 h after IFNγ treatment (personal communication R. Camicia). This is early compared to the reported late increase of p62 transcripts and protein levels in RAW264.7 macrophages after 24 h of IFNγ treatement (138). The same authors also report that p62 negatively regulates the expression of IL-12p40, a subunit of the cytokine IL-12 that shifts CD4+ cell development to a Th1 phenotype (139). This negative feedback loop could contribute to the homeostasis between activation and suppression of innate immunity and prevent adverse consequences like inflammatory disorders and cancer (2) that are related to unrestrained activation of ARTD9/BAL1 dependent signaling and gene expression (44).

In a nutshell, the data presented in this thesis suggest that ARTD9 interacts with p62 over its *macro* domains and is mono-ubiquitinylated. ARTD9 was reduced significantly by 40% after 4 h starvation in a p62 dependent but beclin-1 independent way. Therefore, ARTD9 is most likely degraded by p62 dependent but beclin-1 independent selective autophagy.

5.1 Outlook

PARP (ARTD) inhibitors are already in clinical trials as treatment for cancer (140). ARTD9 levels correlate with chemoresistance in DLBCL, and ARTD8 was shown to protect against IL-4 induced apoptosis (14, 42), but the extent to which BAL proteins contribute to cancer or adverse reactions during its treatment with these inhibitors remains to be further elucidated.

Furthermore, expression of the BAL *macro* domains in insect or mammalian cells and following interaction studies would be interesting to perform and to confirm the interactions found in this study. In addition, the expression of large amounts of the tandem or triplet *macro* domains of BAL proteins and subsequent X-ray crystallography could give structural and functional insights into their mechanism.

In this context, it would be interesting to confirm that the observed decrease of ARTD9 after starvation is indeed due to autophagy. This could be tested in an experiment using siRNA against Atg7 or Atg5, proteins known to inhibit beclin-1 independent autophagy. If confirmed, it would be interesting to investigate the effect of IFNγ, an inducer of autophagy as well as ARTD9/BAL1.

Of note, SUDHL7, the cell line where high ARTD9/BAL1 levels were detected (15), is reported on the Sanger Institute Catalogue Of Somatic Mutations In Cancer to have a mutation in PTEN (141). As described in the introduction, loss-of-function mutations in PTEN can activate mTORC1 and inhibit autophagy. This might be an explanation for the high ARTD9 levels observed in this cell line.

Another question to prove is, how ARTD9 and p62 interact. p62 binds to mono-ubiquitinylated proteins as published previously and a subfraction of ARTD9 was shown to be mono-ubiquitinylated in this study. On the other hand it would be very interesting to investigate if p62 is ADP-ribosylated, since it interacts with the *macro* domains of ARTD9. Since ARTD9 was published to be catalytically inactive other enzymes would have to ADP-ribosylate p62 (43). In this screen ARTD1, ARTD8 and ARTD13 were identified as interaction partners of ARTD9. Like ARTD9, ARTD13 is thought to be inactive, but ARTD1 and ARTD8 would be interesting candidates (17). A first hint in this direction could be, that LPS and H_2O_2 treatment reduced the interaction between ARTD9 and p62 (Fig. 16 and 17).

Last but not least it would be interesting to investigate, if other ARTD proteins are degraded by autophagy or influence autophagy.

References

[1] Lodish, H., Berk, A., Kaiser, C. A., Krieger, M., Scott, M. P., Bretscher, A., Ploegh, H., and Matsudaira, P. (2007) Molecular Cell Biology, W. H. Freeman, 6th edition.

[2] Karin, M., Lawrence, T., and Nizet, V. (2006) Innate immunity gone awry: linking microbial infections to chronic inflammation and cancer. *Cell,* **124**(4), 823–835.

[3] Corda, D. and Di Girolamo, M. (2002) Mono-ADP-ribosylation: a tool for modulating immune response and cell signaling. *Science's STKE,* **2002**(163), pe53.

[4] Hassa, P. O. and Hottiger, M. O. (2008) The diverse biological roles of mammalian PARPS, a small but powerful family of poly-ADP-ribose polymerases.. *Frontiers in bioscience: a journal and virtual library,* **13**, 3046.

[5] Deribe, Y. L., Pawson, T., and Dikic, I. (2010) Post-translational modifications in signal integration. *Nature structural & molecular biology,* **17**(6), 666–672.

[6] Levine, B., Mizushima, N., and Virgin, H. W. (2011) Autophagy in immunity and inflammation. *Nature,* **469**(7330), 323–335.

[7] Saitoh, T. and Akira, S. (2010) Regulation of innate immune responses by autophagy-related proteins. *The Journal of cell biology,* **189**(6), 925–935.

[8] Deretic, V. (2005) Autophagy in innate and adaptive immunity. *Trends in immunology,* **26**(10), 523–528.

[9] Deretic, V. and Levine, B. (2009) Autophagy, immunity, and microbial adaptations. *Cell host & microbe,* **5**(6), 527–549.

[10] van der Heden van Noort, G. J., van der Horst, M. G., Overkleeft, H. S., van der Marel, G. A., and Filippov, D. V. (2010) Synthesis of Mono-ADP-Ribosylated Oligopeptides Using Ribosylated Amino Acid Building Blocks. *Journal of the American Chemical Society,* **132**(14), 5236–5240.

[11] Hassa, P., Haenni, S., Elser, M., and Hottiger, M. (2006) Nuclear ADP-ribosylation reactions in mammalian cells: where are we today and where are we going?. *Microbiology and molecular biology reviews,* **70**(3), 789.

[12] Hottiger, M. O., Hassa, P. O., Lüscher, B., Schüler, H., and Koch-Nolte, F. (2010) Toward a unified nomenclature for mammalian ADP-ribosyltransferases. *Trends in Biochemical Sciences,* **35**(4), 208–219.

[13] Otto, H., Reche, P., Bazan, F., Dittmar, K., Haag, F., and Koch-Nolte, F. (2005) In silico characterization of the family of PARP-like poly (ADP-ribosyl) transferases (pARTs). *BMC genomics,* **6**(1), 139.

[14] Aguiar, R. C. T., Takeyama, K., He, C., Kreinbrink, K., and Shipp, M. A. (2005) B-aggressive lymphoma family proteins have unique domains that modulate transcription and exhibit poly (ADP-ribose) polymerase activity. *Journal of Biological Chemistry,* **280**(40), 33756.

[15] Aguiar, R. C. T., Yakushijin, Y., Kharbanda, S., Salgia, R., Fletcher, J. A., and Shipp, M. A. (2000) BAL is a novel risk-related gene in diffuse large B-cell lymphomas that enhances cellular migration. *Blood,* **96**(13), 4328.

[16] Hakmé, A., Huber, A., Dollé, P., and Schreiber, V. (2008) The macroPARP genes Parp-9 and Parp-14 are developmentally and differentially regulated in mouse tissues. *Developmental Dynamics,* **237**(1), 209–215.

[17] Kleine, H., Poreba, E., Lesniewicz, K., Hassa, P. O., Hottiger, M. O., Litchfield, D. W., Shilton, B. H., and Lüscher, B. (2008) Substrate-assisted catalysis by PARP10 limits its activity to mono-ADP-ribosylation. *Molecular Cell,* **32**(1), 57–69.

[18] Leung, A. K., Vyas, S., Rood, J. E., Bhutkar, A., Sharp, P. A., Chang, P., et al. (2011) Poly (ADP-ribose) regulates stress responses and microRNA activity in the cytoplasm.. *Molecular cell,* **42**(4), 489.

[19] Aravind, L. (2001) The WWE domain: a common interaction module in protein ubiquitination and ADP ribosylation. *Trends in Biochemical Sciences,* **26**(5), 273–275.

[20] Wang, Z., Michaud, G. A., Cheng, Z., Zhang, Y., Hinds, T. R., Fan, E., Cong, F., and Xu, W. (2012) Recognition of the iso-ADP-ribose moiety in poly (ADP-ribose) by WWE domains suggests a general mechanism for poly (ADP-ribosyl) ation-dependent ubiquitination. *Science's STKE,* **26**(3), 235.

[21] Dominguez, G., Wang, C. Y., and Frey, T. K. (1990) Sequence of the genome RNA of rubella virus: Evidence for genetic rearrangement during togavirus evolution. *Virology,* **177**(1), 225–238.

[22] Gorbalenya, A. E., Koonin, E. V., and Lai, M. M. C. (1991) Putative papain-related thiol proteases of positive-strand RNA viruses Identification of rubi-and aphthovirus proteases and delineation of a novel conserved domain associated with proteases of rubi-, α-and coronaviruses. *FEBS Letters,* **288**(1-2), 201–205.

[23] Angelov, D., Molla, A., Perche, P. Y., Hans, F., Coté, J., Khochbin, S., Bouvet, P., and Dimitrov, S. (2003) The histone variant macroH2A interferes with transcription factor binding and SWI/SNF nucleosome remodeling. *Molecular Cell,* **11**(4), 1033–1041.

[24] Pehrson, J. R. and Fried, V. A. (1992) MacroH2A, a core histone containing a large nonhistone region. *Science,* **257**(5075), 1398.

[25] Pehrson, J. R. and Fuji, R. N. (1998) Evolutionary conservation of histone macroH2A subtypes and domains. *Nucleic Acids Research,* **26**(12), 2837.

[26] Martzen, M. R., McCraith, S. M., Spinelli, S. L., Torres, F. M., Fields, S., Grayhack, E. J., and Phizicky, E. M. (1999) A biochemical genomics approach for identifying genes by the activity of their products. *Science,* **286**(5442), 1153.

[27] Allen, M. D., Buckle, A. M., Cordell, S. C., Löwe, J., and Bycroft, M. (2003) The crystal structure of AF1521 a protein from Archaeoglobus fulgidus with homology to the non-histone domain of macroH2A. *Journal of Molecular Biology,* **330**(3), 503–511.

[28] Shull, N. P., Spinelli, S. L., and Phizicky, E. M. (2005) A highly specific phosphatase that acts on ADP-ribose 1"-phosphate, a metabolite of tRNA splicing in Saccharomyces cerevisiae. *Nucleic acids research,* **33**(2), 650.

[29] Neuvonen, M. and Ahola, T. (2009) Differential activities of cellular and viral macro domain proteins in binding of ADP-ribose metabolites. *Journal of Molecular Biology,* **385**(1), 212–225.

[30] Peterson, F. C., Chen, D., Lytle, B. L., Rossi, M. N., Ahel, I., Denu, J. M., and Volkman, B. F. (2011) Orphan Macrodomain Protein (Human C6orf130) Is an O-Acyl-ADP-ribose Deacylase. *Journal of Biological Chemistry,* **286**(41), 35955–35965.

[31] Snijder, E. J., Bredenbeek, P. J., Dobbe, J. C., Thiel, V., Ziebuhr, J., Poon, L. L. M., Guan, Y., Rozanov, M., Spaan, W. J. M., and Gorbalenya, A. E. (2003) Unique and conserved features of genome and proteome of SARS-coronavirus, an early split-off from the coronavirus group 2 lineage. *Journal of Molecular Biology,* **331**(5), 991–1004.

[32] Egloff, M. P., Malet, H., Putics, Á., Heinonen, M., Dutartre, H., Frangeul, A., Gruez, A., Campanacci, V., Cambillau, C., Ziebuhr, J., et al. (2006) Structural and functional basis for ADP-ribose and poly (ADP-ribose) binding by viral macro domains. *Journal of Virology,* **80**(17), 8493.

[33] Karras, G. I., Kustatscher, G., Buhecha, H. R., Allen, M. D., Pugieux, C., Sait, F., Bycroft, M., and Ladurner, A. G. (2005) The macro domain is an ADP-ribose binding module. *The EMBO Journal,* **24**(11), 1911–1920.

[34] Gamble, M. J. and Kraus, W. L. (2010) Multiple facets of the unique histone variant macroH2A: From genomics to cell biology. *Cell cycle,* **9**(13).

[35] Kustatscher, G., Hothorn, M., Pugieux, C., Scheffzek, K., and Ladurner, A. G. (2005) Splicing regulates NAD metabolite binding to histone macroH2A. *Nature Structural & Molecular Biology,* **12**(7), 624–625.

[36] Ahel, D., Horejsi, Z., Wiechens, N., Polo, S. E., Garcia-Wilson, E., Ahel, I., Flynn, H., Skehel, M., West, S. C., Jackson, S. P., et al. (2009) Poly (ADP-ribose)-dependent regulation of DNA repair by the chromatin remodeling enzyme ALC1. *Science,* **325**(5945), 1240.

[37] Dani, N., Stilla, A., Marchegiani, A., Tamburro, A., Till, S., Ladurner, A. G., Corda, D., and Di Girolamo, M. (2009) Combining affinity purification by ADP-ribose-binding macro domains with mass spectrometry to define the mammalian ADP-ribosyl proteome. *Proceedings of the National Academy of Sciences,* **106**(11), 4243.

[38] Gottschalk, A. J., Timinszky, G., Kong, S. E., Jin, J., Cai, Y., Swanson, S. K., Washburn, M. P., Florens, L., Ladurner, A. G., Conaway, J. W., and Conaway, R. C. (2009) Poly(ADP-ribosyl)ation directs recruitment and activation of an ATP-dependent chromatin remodeler. *Proceedings of the National Academy of Sciences,* **106**(33), 13770–13774.

[39] Baus, D., Nonnenmacher, F., Jankowski, S., Döring, C., Bräutigam, C., Frank, M., Hansmann, M. L., and Pfitzner, E. (2009) STAT6 and STAT1 are essential antagonistic regulators of cell survival in classical Hodgkin lymphoma cell line. *Leukemia,* **23**(10), 1885–1893.

[40] Goenka, S. and Boothby, M. (2006) Selective potentiation of Stat-dependent gene expression by collaborator of Stat6 (CoaSt6), a transcriptional cofactor. *Proceedings of the National Academy of Sciences,* **103**(11), 4210–4215.

[41] Mehrotra, P., Riley, J., Patel, R., Li, F., Voss, L., and Goenka, S. (2010) PARP-14 functions as a transcriptional switch for STAT6 dependent gene activation. *Journal of Biological Chemistry,*.

[42] Cho, S. H., Goenka, S., Henttinen, T., Gudapati, P., Reinikainen, A., Eischen, C. M., Lahesmaa, R., and Boothby, M. (2009) PARP-14, a member of the B aggressive lymphoma family, transduces survival signals in primary B cells. *Blood,* **113**(11), 2416.

[43] Juszczynski, P., Kutok, J. L., Li, C., Mitra, J., Aguiar, R. C. T., and Shipp, M. A. (2006) BAL1 and BBAP are regulated by a gamma interferon-responsive bidirectional promoter and are overexpressed in diffuse large B-cell lymphomas with a prominent inflammatory infiltrate. *Molecular and Cellular Biology,* **26**(14), 5348.

[44] Camicia, R. and Bachmann, S. B. and Winkler, H. C. and Hassa, P. O. B-aggressive lymphoma protein BAL1/ARTD9 inhibits tumor suppressor IRF1 and activates oncogene BCL6 to mediate survival in diffuse large B-cell lymphoma. Submitted.

[45] Nelms, K., Keegan, A. D., Zamorano, J., Ryan, J. J., and Paul, W. E. (1999) The IL-4 receptor: signaling mechanisms and biologic functions. *Annual Review of Immunology,* **17**(1), 701–738.

[46] Shuai, K. and Liu, B. (2003) Regulation of JAK–STAT signalling in the immune system. *Nature Reviews Immunology,* **3**(11), 900–911.

[47] Darnell Jr, J. E. (1997) STATs and gene regulation. *Science,* **277**(5332), 1630.

[48] Mosmann, T. R. and Sad, S. (1996) The expanding universe of T-cell subsets: Th1, Th2 and more. *Immunology Today,* **17**(3), 138–146.

[49] Aaronson, D. S. and Horvath, C. M. (2002) A road map for those who don't know JAK-STAT. *Science,* **296**(5573), 1653.

[50] Liu, K. D., Gaffen, S. L., and Goldsmith, M. A. (1998) JAK/STAT signaling by cytokine receptors. *Current opinion in immunology,* **10**(3), 271–278.

[51] Taniguchi, T., Ogasawara, K., Takaoka, A., and Tanaka, N. (2001) IRF family of transcription factors as regulators of host defense. *Annual review of immunology,* **19**(1), 623–655.

[52] Shi, L., Perin, J. C., Leipzig, J., Zhang, Z., and Sullivan, K. E. (2011) Genome-wide analysis of interferon regulatory factor I binding in primary human monocytes. *Gene,*.

[53] Romeo, G., Fiorucci, G., Chiantore, M. V., Percario, Z. A., Vannucchi, S., and Affabris, E. (2002) Review: IRF-1 as a negative regulator of cell proliferation. *Journal of interferon & cytokine research,* **22**(1), 39–47.

[54] Yoshimura, A., Naka, T., and Kubo, M. (2007) SOCS proteins, cytokine signalling and immune regulation. *Nature Reviews Immunology,* **7**(6), 454–465.

[55] Shuai, K. (2000) Modulation of STAT signaling by STAT-interacting proteins. *Oncogene,* **19**(21), 2638–2644.

[56] Tanaka, T., Soriano, M. A., and Grusby, M. J. (2005) SLIM is a nuclear ubiquitin E3 ligase that negatively regulates STAT signaling. *Immunity,* **22**(6), 729–736.

[57] Schindler, C., Levy, D. E., and Decker, T. (2007) JAK-STAT signaling: from interferons to cytokines. *Journal of Biological Chemistry,* **282**(28), 20059.

[58] Lenz, G. and Staudt, L. M. (2010) Aggressive lymphomas. *New England Journal of Medicine,* **362**(15), 1417–1429.

[59] Hanahan, D. and Weinberg, R. A. (2011) Hallmarks of cancer: the next generation. *Cell,* **144**(5), 646–674.

[60] Kumar, V., Abbas, A. K., Fausto, N., and Aster, J. (2009) Robbins and Cotran Pathologic Basis of Disease, Professional Edition, Saunders, 8th edition.

[61] Ferlay, J., Shin, H. R., Bray, F., Forman, D., Mathers, C., and Parkin, D. M. (2010) Estimates of worldwide burden of cancer in 2008: GLOBOCAN 2008. *International Journal of Cancer,* **127**, 2893–2917.

[62] Coussens, L. M. and Werb, Z. (2002) Inflammation and cancer. *Nature,* **420**(6917), 860–867.

[63] Roman, E. and Smith, A. G. (2011) Epidemiology of lymphomas. *Histopathology,* **58**(1), 4–14.

[64] Murawski, N. and Pfreundschuh, M. (2010) New drugs for aggressive B-cell and T-cell lymphomas. *The Lancet Oncology,* **11**(11), 1074–1085.

[65] Alizadeh, A. A., Eisen, M. B., Davis, R. E., Ma, C., Lossos, I. S., Rosenwald, A., Boldrick, J. C., Sabet, H., Tran, T., Yu, X., et al. (2000) Distinct types of diffuse large B-cell lymphoma identified by gene expression profiling. *Nature,* **403**(6769), 503–511.

[66] Rosenwald, A., Wright, G., Chan, W. C., Connors, J. M., Campo, E., Fisher, R. I., Gascoyne, R. D., Muller-Hermelink, H. K., Smeland, E. B., Giltnane, J. M., et al. (2002) The use of molecular profiling to predict survival after chemotherapy for diffuse large-B-cell lymphoma. *New England Journal of Medicine,* **346**(25), 1937.

[67] Sarosiek, K. A., Nechushtan, H., Lu, X., Rosenblatt, J. D., and Lossos, I. S. (2009) Interleukin-4 distinctively modifies responses of germinal centre-like and activated B-cell-like diffuse large B-cell lymphomas to immuno-chemotherapy. *British Journal of Haematology,* **147**(3), 308–318.

[68] Lu, X., Nechushtan, H., Ding, F., Rosado, M. F., Singal, R., Alizadeh, A. A., and Lossos, I. S. (2005) Distinct IL-4-induced gene expression, proliferation, and intracellular signaling in germinal center B-cell-like and activated B-cell-like diffuse large-cell lymphomas. *Blood,* **105**(7), 2924.

[69] Johansen, T. and Lamark, T. (2011) Selective autophagy mediated by autophagic adapter proteins. *Autophagy,* **7**(3), 279.

[70] Mizushima, N., Levine, B., Cuervo, A. M., and Klionsky, D. J. (2008) Autophagy fights disease through cellular self-digestion. *Nature,* **451**(7182), 1069–1075.

[71] Xie, Z. and Klionsky, D. J. (2007) Autophagosome formation: core machinery and adaptations. *Nature cell biology,* **9**(10), 1102–1109.

[72] Levine, B. and Kroemer, G. (2008) Autophagy in the pathogenesis of disease. *Cell,* **132**(1), 27–42.

[73] Mizushima, N. and Komatsu, M. (2011) Autophagy: renovation of cells and tissues. *Cell,* **147**(4), 728–741.

[74] Backer, J. M., Bourret, L., and Dice, J. F. (1983) Regulation of catabolism of microinjected ribonuclease A requires the amino-terminal 20 amino acids. *Proceedings of the National Academy of Sciences,* **80**(8), 2166.

[75] Wing, S. S., Chiang, H. L., Goldberg, A. L., and Dice, J. F. (1991) Proteins containing peptide sequences related to Lys-Phe-Glu-Arg-Gln are selectively depleted in liver and heart, but not skeletal muscle, of fasted rats.. *Biochemical journal,* **275**(Pt 1), 165.

[76] Kroemer, G., Mariño, G., and Levine, B. (2010) Autophagy and the integrated stress response. *Molecular cell,* **40**(2), 280–293.

[77] Harris, J., Master, S., De Haro, S., Delgado, M., Roberts, E., Hope, J., Keane, J., and Deretic, V. (2009) Th1-Th2 polarisation and autophagy in the control of intracellular mycobacteria by macrophages. *Veterinary immunology and immunopathology,* **128**(1-3), 37–43.

[78] Feng, C. G., Zheng, L., Jankovic, D., Báfica, A., Cannons, J. L., Watford, W. T., Chaussabel, D., Hieny, S., Caspar, P., Schwartzberg, P. L., et al. (2008) The immunity-related GTPase Irgm1 promotes the expansion of activated CD4+ T cell populations by preventing interferon-γ-induced cell death. *Nature immunology,* **9**(11), 1279–1287.

[79] Khalkhali-Ellis, Z., Abbott, D. E., Bailey, C. M., Goossens, W., Margaryan, N. V., Gluck, S. L., Reuveni, M., and Hendrix, M. J. C. (2008) IFN-γ regulation of vacuolar pH, cathepsin D processing and autophagy in mammary epithelial cells. *Journal of cellular biochemistry,* **105**(1), 208–218.

[80] Pyo, J. O., Jang, M. H., Kwon, Y. K., Lee, H. J., Jun, J. I. L., Woo, H. N., Cho, D. H., Choi, B. Y., Lee, H., Kim, J. H., et al. (2005) Essential roles of Atg5 and FADD in autophagic cell death. *Journal of Biological Chemistry,* **280**(21), 20722–20729.

[81] Yu, L., McPhee, C. K., Zheng, L., Mardones, G. A., Rong, Y., Peng, J., Mi, N., Zhao, Y., Liu, Z., Wan, F., et al. (2010) Termination of autophagy and reformation of lysosomes regulated by mTOR. *Nature,* **465**(7300), 942–946.

[82] Duran, A., Amanchy, R., Linares, J. F., Joshi, J., Abu-Baker, S., Porollo, A., Hansen, M., Moscat, J., and Diaz-Meco, M. T. (2011) p62 is a key regulator of nutrient sensing in the mTORC1 pathway. *Molecular cell,* **44**(1), 134–146.

[83] Hay, N. and Sonenberg, N. (2004) Upstream and downstream of mTOR. *Genes & development,* **18**(16), 1926–1945.

[84] Sabatini, D. M. (2006) mTOR and cancer: insights into a complex relationship. *Nature Reviews Cancer,* **6**(9), 729–734.

[85] Cantley, L. C. and Neel, B. G. (1999) New insights into tumor suppression: PTEN suppresses tumor formation by restraining the phosphoinositide 3-kinase/AKT pathway. *Proceedings of the National Academy of Sciences,* **96**(8), 4240.

[86] Simpson, L. and Parsons, R. (2001) PTEN: life as a tumor suppressor. *Experimental cell research,* **264**(1), 29–41.

[87] Cell Signaling Technology, Inc. Autophagy Signaling Diagram, accessed 2012–03–25. http://www.cellsignal.com.

[88] Nakatogawa, H., Suzuki, K., Kamada, Y., and Ohsumi, Y. (2009) Dynamics and diversity in autophagy mechanisms: lessons from yeast. *Nature Reviews Molecular Cell Biology,* **10**(7), 458–467.

[89] Itakura, E. and Mizushima, N. (2010) Characterization of autophagosome formation site by a hierarchical analysis of mammalian Atg proteins.. *Autophagy,* **6**(6), 764.

[90] Suzuki, K., Kubota, Y., Sekito, T., and Ohsumi, Y. (2007) Hierarchy of Atg proteins in pre-autophagosomal structure organization. *Genes to Cells,* **12**(2), 209–218.

[91] Fujita, N., Itoh, T., Omori, H., Fukuda, M., Noda, T., and Yoshimori, T. (2008) The Atg16L complex specifies the site of LC3 lipidation for membrane biogenesis in autophagy. *Molecular biology of the cell,* **19**(5), 2092–2100.

[92] Weidberg, H., Shvets, E., Shpilka, T., Shimron, F., Shinder, V., and Elazar, Z. (2010) LC3 and GATE-16/GABARAP subfamilies are both essential yet act differently in autophagosome biogenesis. *The EMBO journal,* **29**(11), 1792–1802.

[93] Mizushima, N., Yoshimori, T., et al. (2007) How to interpret LC3 immunoblotting. *Autophagy,* **3**(6), 542.

[94] Klionsky, D. J., Abeliovich, H., Agostinis, P., Agrawal, D. K., Aliev, G., Askew, D. S., Baba, M., Baehrecke, E. H., Bahr, B. A., Ballabio, A., et al. (2008) Guidelines for the use and interpretation of assays for monitoring autophagy in higher eukaryotes. *Autophagy,* **4**(2), 151.

[95] Bjørkøy, G., Lamark, T., Brech, A., Outzen, H., Perander, M., Øvervatn, A., Stenmark, H., and Johansen, T. (2005) p62/SQSTM1 forms protein aggregates degraded by autophagy and has a protective effect on huntingtin-induced cell death. *The Journal of cell biology,* **171**(4), 603–614.

[96] Pankiv, S., Clausen, T. H., Lamark, T., Brech, A., Bruun, J. A., Outzen, H., Øvervatn, A., Bjørkøy, G., and Johansen, T. (2007) p62/SQSTM1 binds directly to Atg8/LC3 to facilitate degradation of ubiquitinated protein aggregates by autophagy. *Journal of Biological Chemistry,* **282**(33), 24131–24145.

[97] Chiang, H. L. and Dice, J. F. (1988) Peptide sequences that target proteins for enhanced degradation during serum withdrawal.. *Journal of Biological Chemistry,* **263**(14), 6797–6805.

[98] Chiang, H. L., Terlecky, S. R., Plant, C. P., Dice, J. F., et al. (1989) A role for a 70-kilodalton heat shock protein in lysosomal degradation of intracellular proteins. *Science,* **246**(4928), 382–385.

[99] Cuervo, A. M. (2010) Chaperone-mediated autophagy: selectivity pays off. *Trends in Endocrinology & Metabolism,* **21**(3), 142–150.

[100] Kon, M., Kiffin, R., Koga, H., Chapochnick, J., Macian, F., Varticovski, L., and Cuervo, A. M. (2011) Chaperone-Mediated Autophagy Is Required for Tumor Growth. *Science Translational Medicine,* **3**(109), 109ra117–109ra117.

[101] Ichimura, Y., Kumanomidou, T., Sou, Y., Mizushima, T., Ezaki, J., Ueno, T., Kominami, E., Yamane, T., Tanaka, K., and Komatsu, M. (2008) Structural basis for sorting mechanism of p62 in selective autophagy. *Journal of Biological Chemistry,* **283**(33), 22847–22857.

[102] Komatsu, M., Waguri, S., Koike, M., Sou, Y., Ueno, T., Hara, T., Mizushima, N., Iwata, J., Ezaki, J., Murata, S., et al. (2007) Homeostatic levels of p62 control cytoplasmic inclusion body formation in autophagy-deficient mice. *Cell,* **131**(6), 1149–1163.

[103] Zatloukal, K., Stumptner, C., Fuchsbichler, A., Heid, H., Schnoelzer, M., Kenner, L., Kleinert, R., Prinz, M., Aguzzi, A., and Denk, H. (2002) p62 Is a common component of cytoplasmic inclusions in protein aggregation diseases. *The American journal of pathology,* **160**(1), 255.

[104] Vadlamudi, R. K., Joung, I., Strominger, J. L., and Shin, J. (1996) p62, a phosphotyrosine-independent ligand of the SH2 domain of p56lck, belongs to a new class of ubiquitin-binding proteins. *Journal of Biological Chemistry,* **271**(34), 20235.

[105] Kirkin, V., Lamark, T., Sou, Y., Bjørkøy, G., Nunn, J., Bruun, J., Shvets, E., McEwan, D., Clausen, T., Wild, P., et al. (2009) A role for NBR1 in autophagosomal degradation of ubiquitinated substrates. *Molecular cell,* **33**(4), 505–516.

[106] Cavey, J., Ralston, S., Hocking, L., Sheppard, P., Ciani, B., Searle, M., and Layfield, R. (2005) Loss of Ubiquitin-Binding Associated With Paget's Disease of Bone p62 (SQSTM1) Mutations. *Journal of Bone and Mineral Research,* **20**(4), 619–624.

[107] Kim, P. K., Hailey, D. W., Mullen, R. T., and Lippincott-Schwartz, J. (2008) Ubiquitin signals autophagic degradation of cytosolic proteins and peroxisomes. *Proceedings of the National Academy of Sciences,* **105**(52), 20567–20574.

[108] Takeyama, K., Aguiar, R. C. T., Gu, L., He, C., Freeman, G. J., Kutok, J. L., Aster, J. C., and Shipp, M. A. (2003) The BAL-binding protein BBAP and related Deltex family members exhibit ubiquitin-protein isopeptide ligase activity. *Journal of Biological Chemistry,* **278**(24), 21930.

[109] Goenka, S., Cho, S. H., and Boothby, M. (2007) Collaborator of Stat6 (CoaSt6)-associated poly (ADP-ribose) polymerase activity modulates Stat6-dependent gene transcription. *Journal of Biological Chemistry,* **282**(26), 18732.

[110] Yanagawa, T., Funasaka, T., Tsutsumi, S., Hu, H., Watanabe, H., and Raz, A. (2007) Regulation of phosphoglucose isomerase/autocrine motility factor activities by the poly (ADP-ribose) polymerase family-14. *Cancer Research,* **67**(18), 8682.

[111] Timinszky, G., Till, S., Hassa, P. O., Hothorn, M., Kustatscher, G., Nijmeijer, B., Colombelli, J., Altmeyer, M., Stelzer, E. H. K., Scheffzek, K., Hottiger, M. O., and Ladurner, A. G. (2009) A macrodomain-containing histone rearranges chromatin upon sensing PARP1 activation. *Nature Structural & Molecular Biology,* **16**(9), 923–929.

[112] Fritsch, E. F., Sambrook, J., and Maniatis, T. (2001) Molecular Cloning, a Laboratory Manual, Cold Spring Harbor Laboratory, 3rd edition.

[113] Kawamitsu, H., Hoshino, H., Okada, H., Miwa, M., Momoi, H., and Sugimura, T. (1984) Monoclonal antibodies to poly (adenosine diphosphate ribose) recognize different structures. *Biochemistry,* **23**(16), 3771–3777.

[114] Amini, R. M., Berglund, M., Rosenquist, R., Von Heideman, A., Lagercrantz, S., Thunberg, U., Bergh, J., Sundström, C., Glimelius, B., and Enblad, G. (2002) A novel B-cell line (U-2932) established from a patient with diffuse large B-cell lymphoma following Hodgkin lymphoma. *Leukemia & lymphoma,* **43**(11), 2179–2189.

[115] Orvedahl, A., MacPherson, S., Sumpter Jr, R., Tallóczy, Z., Zou, Z., and Levine, B. (2010) Autophagy protects against Sindbis virus infection of the central nervous system. *Cell host & microbe,* **7**(2), 115–127.

[116] Glatter, T., Wepf, A., Aebersold, R., and Gstaiger, M. (2009) An integrated workflow for charting the human interaction proteome: insights into the PP2A system. *Molecular Systems Biology,* **5**(1).

[117] Candiano, G., Bruschi, M., Musante, L., Santucci, L., Ghiggeri, G. M., Carnemolla, B., Orecchia, P., Zardi, L., and Righetti, P. G. (2004) Blue silver: A very sensitive colloidal Coomassie G-250 staining for proteome analysis. *Electrophoresis,* **25**(9), 1327–1333.

[118] Keller, A., Nesvizhskii, A. I., Kolker, E., and Aebersold, R. (2002) Empirical statistical model to estimate the accuracy of peptide identifications made by MS/MS and database search. *Analytical chemistry,* **74**(20), 5383–5392.

[119] Nesvizhskii, A. I., Keller, A., Kolker, E., and Aebersold, R. (2003) A statistical model for identifying proteins by tandem mass spectrometry. *Analytical chemistry,* **75**(17), 4646–4658.

[120] Moretti, S., Armougom, F., Wallace, I. M., Higgins, D. G., Jongeneel, C. V., and Notredame, C. (2007) The M-Coffee web server: a meta-method for computing multiple sequence alignments by combining alternative alignment methods. *Nucleic acids research,* **35**(suppl 2), W645–W648.

[121] Wallace, I. M., O'Sullivan, O., Higgins, D. G., and Notredame, C. (2006) M-Coffee: combining multiple sequence alignment methods with T-Coffee. *Nucleic acids research,* **34**(6), 1692–1699.

[122] Notredame, C., Higgins, D. G., Heringa, J., et al. (2000) T-Coffee: A novel method for fast and accurate multiple sequence alignment. *Journal of molecular biology,* **302**(1), 205–218.

[123] Kelley, L. A. and Sternberg, M. J. E. (2009) Protein structure prediction on the Web: a case study using the Phyre server. *Nature Protocols,* **4**(3), 363–371.

[124] Ezkurdia, I., Graña, O., Izarzugaza, J. M. G., and Tress, M. L. (2009) Assessment of domain boundary predictions and the prediction of intramolecular contacts in CASP8. *Proteins: Structure, Function, and Bioinformatics,* **77**(S9), 196–209.

[125] Schrödinger, LLC (August, 2010) The PyMOL Molecular Graphics System, Version 1.3r1.

[126] Xu, J. and Zhang, Y. (2010) How significant is a protein structure similarity with TM-score= 0.5?. *Bioinformatics,* **26**(7), 889.

[127] Amir-Zaltsman, Y., Ezra, E., Scherson, T., Zutra, A., Littauer, U. Z., and Salomon, Y. (1982) ADP-ribosylation of microtubule proteins as catalyzed by cholera toxin.. *The EMBO journal,* **1**(2), 181.

[128] Leitinger, N. and Wesierska-Gadek, J. (1993) ADP-ribosylation of nucleolar proteins in HeLa tumor cells. *Journal of cellular biochemistry,* **52**(2), 153–158.

[129] Lai, J. S. and Herr, W. (1992) Ethidium bromide provides a simple tool for identifying genuine DNA-independent protein associations. *Proceedings of the National Academy of Sciences,* **89**(15), 6958.

[130] Gao, G., Guo, X., and Goff, S. P. (2002) Inhibition of retroviral RNA production by ZAP, a CCCH-type zinc finger protein. *Science,* **297**(5587), 1703–1706.

[131] Bick, M. J., Carroll, J. W. N., Gao, G., Goff, S. P., Rice, C. M., and MacDonald, M. R. (2003) Expression of the zinc-finger antiviral protein inhibits alphavirus replication. *Journal of virology,* **77**(21), 11555–11562.

[132] Sbodio, J. I., Lodish, H. F., and Chi, N. W. (2002) Tankyrase-2 oligomerizes with tankyrase-1 and binds to both TRF1 (telomere-repeat-binding factor 1) and IRAP (insulin-responsive aminopeptidase).. *Biochemical Journal,* **361**(Pt 3), 451.

[133] Schreiber, V., Amé, J. C., Dollé, P., Schultz, I., Rinaldi, B., Fraulob, V., Ménissier-de Murcia, J., and de Murcia, G. (2002) Poly (ADP-ribose) polymerase-2 (PARP-2) is required for efficient base excision DNA repair in association with PARP-1 and XRCC1. *Journal of Biological Chemistry,* **277**(25), 23028–23036.

[134] Schwientek, M. S., Higgins, L. A., and Fallon, A. M. (2002) Cultured Aedes albopictus mosquito cells accumulate elongation factor-1 [alpha](EF-1 [alpha]) during serum starvation. *Insect biochemistry and molecular biology,* **32**(9), 1055–1063.

[135] Lichtenstein, A., Minogue, P. J., Beyer, E. C., and Berthoud, V. M. (2011) Autophagy: a pathway that contributes to connexin degradation. *Journal of Cell Science,* **124**(6), 910–920.

[136] Moscat, J. and Diaz-Meco, M. T. (2009) p62 at the crossroads of autophagy, apoptosis, and cancer. *Cell,* **137**(6), 1001–1004.

[137] Paul, S., Kashyap, A. K., Jia, W., He, Y. W., and Schaefer, B. C. (2012) Selective Autophagy of the Adaptor Protein Bcl10 Modulates T Cell Receptor Activation of NF-κB. *Immunity,* doi:10.1016/j.immuni.2012.04.008.

[138] Kim, J. Y. and Ozato, K. (2009) The sequestosome 1/p62 attenuates cytokine gene expression in activated macrophages by inhibiting IFN regulatory factor 8 and TNF receptor-associated factor 6/NF-κB activity. *The Journal of Immunology,* **182**(4), 2131–2140.

[139] Schroder, K., Hertzog, P. J., Ravasi, T., and Hume, D. A. (2004) Interferon-γ: an overview of signals, mechanisms and functions. *Journal of leukocyte biology,* **75**(2), 163–189.

[140] Kummar, S., Kinders, R., Gutierrez, M. E., Rubinstein, L., Parchment, R. E., Phillips, L. R., Ji, J., Monks, A., Low, J. A., Chen, A., et al. (2009) Phase 0 clinical trial of the poly (ADP-ribose) polymerase inhibitor ABT-888 in patients with advanced malignancies. *Journal of Clinical Oncology,* **27**(16), 2705.

[141] Bamford, S., Dawson, E., Forbes, S., Clements, J., Pettett, R., Dogan, A., Flanagan, A., Teague, J., Futreal, P. A., Stratton, M. R., et al. (2004) The COSMIC (Catalogue of Somatic Mutations in Cancer) database and website. *British journal of cancer,* **91**(2), 355–358.

Curriculum Vitae

Name	Hans Christian Winkler
Date of birth	March 8, 1986
Place of birth	Winterthur, ZH
Place of origin	Zürich, ZH and Basel, BS

11/2011–5/2012	**Thesis work** under the supervision of Dr. Paul O. Hassa, Institute of Veterinary Biochemistry and Molecular Biology, Vetsuisse Faculty, University of Zurich
8/2011–10/2011	**Staatsexamen in Veterinary Medicine**
8/2010–1/2011 **3/2010–4/2010**	**Experimental work** under the supervision of Dr. Paul O. Hassa, in the context of the „Schwerpunktfach Biomedizinische Forschung", Institute of Veterinary Biochemistry and Molecular Biology, Vetsuisse Faculty, University of Zurich
6/2009–8/2009	**Leadership Program for Veterinary Students**, Cornell University, Ithaca, USA. Experimental work „Cellular host ranges and tropisms of canine and equine influenza viruses" conducted in the laboratory of Dr. Colin Parrish, Baker Institute
2008–2009	**Immunology teaching assistant (Tutor)** for Prof. Dr. Mark Suter, Immunology, Vetsuisse Faculty, University of Zurich
2007–2010	**Technical assistant** at the Zebrafish hatchery of Prof. Dr. Stephan Neuhauss, Institute of Molecular Life Sciences, University of Zurich
2006–2011	**Course of studies in Veterinary Medicine** at the Vetsuisse Faculty, University of Zurich. Schwerpunktfach Biomedizinische Forschung
7/2006	**Maturität** Maturitätsarbeit „Coffein – Eigenschaften und Wirkungen einer psychotropen Substanz". HPLC analysis and lab work conducted at Novartis AG, Basel
2002–2006	**Alte Kantonsschule Aarau, Aargau** Akzentfach Latein, Schwerpunktfach Biologie und Chemie, Ergänzungsfach Philosophie
1998–2002	**Bezirksschule Frick, Aargau**
1993–1998	**Primary school, Oberhof, Aargau**

Acknowledgments

First, I would like to express my sincere gratitude to Prof. Dr. med. vet. U. Hübscher for giving me the opportunity to carry out this work at the Institute of Veterinary Biochemistry and Molecular Biology.

Special thanks go to Prof. Dr. med. vet et phil. II M. O. Hottiger as Program Director and for personal advice.

I would like to express my gratitude to Dr. P. O. Hassa for giving me the opportunity to work in his laboratory and for his guidance during this project. Thank you for your constant availability when I had questions and for your great support and patience.

Many thanks go to Dr. C. Blenn for collaboration with tools, methodical inputs and many interesting discussions.

A big thank goes to R. Camicia for teaching me various experimental techniques (and some Italian words) and always having time to answer my questions.

Kudos to the Stucki lab for pull-down troubleshooting and daily heat block sharing, to Andrej for PAR detection and Roberta for thought-provoking discussions.

I also would like to highly acknowledge all the other institute members for the friendly atmosphere at the institute.

Above all I would like to thank my family, my dear and incomparable girlfriend Eleni and my colleagues for the continuous support.